Spontaneous and optogenetically induced cortical spreading depolarization in familial hemiplegic migraine type 1 mutant mice

Loonen, I.C.M.; Voskuyl, R.A.; Schenke, M.; Heiningen, S.H. van; Maagdenberg, A.M.J.M. van den; Tolner, E.A.

Neurobiology of Disease 192 (2024) 106405

Contents lists available at ScienceDirect

Neurobiology of Disease

journal homepage: www.elsevier.com/locate/ynbdi

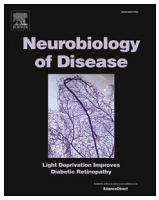

Spontaneous and optogenetically induced cortical spreading depolarization in familial hemiplegic migraine type 1 mutant mice

Inge C.M. Loonen [a], Rob A. Voskuyl [a], Maarten Schenke [a], Sandra H. van Heiningen [a], Arn M.J. M. van den Maagdenberg [a,b,1], Else A. Tolner [a,b,*,1]

[a] Department of Human Genetics, Leiden University Medical Center, Leiden 2333 RC, the Netherlands
[b] Department of Neurology, Leiden University Medical Center, Leiden 2333 RC, the Netherlands

ARTICLE INFO

Keywords:
Behaviour
Cortical excitability
Cortical spreading depolarization
Mouse model
Optogenetics

ABSTRACT

Mechanisms underlying the migraine aura are incompletely understood, which to large extent is related to a lack of models in which cortical spreading depolarization (CSD), the correlate of the aura, occurs spontaneously. Here, we investigated electrophysiological and behavioural CSD features in freely behaving mice expressing mutant $Ca_V2.1$ Ca^{2+} channels, either with the milder R192Q or the severer S218L missense mutation in the α1 subunit, known to cause familial hemiplegic migraine type 1 (FHM1) in patients. Very rarely, spontaneous CSDs were observed in mutant but never in wildtype mice. In homozygous *Cacna1a*^{R192Q} mice exclusively single-wave CSDs were observed whereas heterozygous *Cacna1a*^{S218L} mice displayed multiple-wave events, seemingly in line with the more severe clinical phenotype associated with the S218L mutation. Spontaneous CSDs were associated with body stretching, one-directional slow head turning, and rotating movement of the body. Spontaneous CSD events were compared with those induced in a controlled manner using minimally invasive optogenetics. Also in the optogenetic experiments single-wave CSDs were observed in *Cacna1a*^{R192Q} and *Cacna1a*^{S218L} mice (whereas the latter also showed multiple-wave events) with movements similar to those observed with spontaneous events. Compared to wildtype mice, FHM1 mutant mice exhibited a reduced threshold and an increased propagation speed for optogenetically induced CSD with a more profound CSD-associated dysfunction, as indicated by a prolonged suppression of transcallosal evoked potentials and a reduction of unilateral forepaw grip performance. When induced during sleep, the optogenetic CSD threshold was particularly lowered, which may explain why spontaneous CSD events predominantly occurred during sleep. In conclusion, our data show that key neurophysiological and behavioural features of optogenetically induced CSDs mimic those of rare spontaneous events in FHM1 R192Q and S218L mutant mice with differences in severity in line with FHM1 clinical phenotypes seen with these mutations.

1. Introduction

Migraine is a common brain disorder characterized by attacks of headache and associated neurological symptoms (Headache Classification Committee of the International Headache, 2013). In about one-third of patients the headache phase is typically preceded by an aura, that is likely caused by cortical spreading depolarization (CSD), a wave of intense neuronal and glial activation followed by prolonged suppression of neuronal activity (Leao, 1944; Dreier, 2011), which in animal studies has been shown to activate headache pathways (Zhang et al., 2010; Zhang et al., 2011; Karatas et al., 2013). In the majority of studies, CSD was induced in anesthetized animals that underwent invasive surgery (i.e., drilling burr holes, placing a canula) for KCl application or current injection to induce events (Ayata, 2013; Dreier and Reiffurth, 2015). In freely behaving rats, KCl induced CSD was reported to cause anxiety and various apparent pain-related behaviours, including freezing, head-

Abbreviations: ChR2, channelrhodopsin-2; CSD, cortical spreading depolarization; DC, direct current; ECoG, Electrocorticogram; FHM1, familial hemiplegic migraine type 1; Ir, iridium; M1, primary motor cortex; MUA, multi-unit activity; REM, rapid eye movement; Pt, platinum; S1, primary sensorimotor cortex; TCEP, transcallosal evoked potential; V1, primary visual cortex; WT, wildtype.

* Corresponding author at: Departments of Neurology & Human Genetics; Leiden University Medical Center, Post zone S4-P, Leiden PO Box 9600, the Netherlands.
E-mail address: E.A.Tolner@lumc.nl (E.A. Tolner).

[1] Arn van den Maagdenberg and Else Tolner contributed equally to this work.

https://doi.org/10.1016/j.nbd.2024.106405
Received 30 September 2023; Received in revised form 15 December 2023; Accepted 4 January 2024
Available online 9 January 2024

shaking and wet-dog shakes (Akcali et al., 2010; Tepe et al., 2015; Filiz et al., 2019). More recently, to circumvent the influence of invasive surgery, a minimally invasive optogenetic approach was developed in which light-sensitive channelrhodopsin-2 (ChR2) cation channels expressed in cortical neurons of mice are activated to induce CSD events by shining blue light through the intact skull (Houben et al., 2017; Chung et al., 2019; Tolner et al., 2019). Using optogenetic CSD induction in freely behaving animals, transient freezing, abnormal locomotion, head shaking, and facial grooming was reported, but CSD-associated behaviour was typically studied immediately after (i.e., within 30 min) after induction of CSD (Tang et al., 2020; Harriott et al., 2021; Pi et al., 2022) or without electrophysiological features being recorded (Yousef Yengej et al., 2022). Very recently, we showed that optogenetically induced CSD resulted in a prolonged (depending on the readout hours to several days) headpain-relevant behavioural phenotype, i.e., characterized by increased mouse grimace scale scores and the occurrence of oculotemporal strokes (as measures of pain mimic) and a reduced nest building performance (as a measure of general discomfort) in wildtype mice (Dehghani et al., 2023). Some features of the behavioural phenotype were more pronounced in familial hemiplegic migraine type 1 (FHM1) mutant mice (Dehghani et al., 2023) that expressed the S218L missense mutation in the α1 subunit that results in a gain of function of voltage-gated $Ca_V2.1$ Ca^{2+} channels (Van den Maagdenberg et al., 2010; Vecchia et al., 2015).

To further explore aspects of CSD in relation to neuronal hyperexcitability, we here investigated mutant mice that express either the R192Q or the S218L missense mutation (Van den Maagdenberg et al., 2004; Van den Maagdenberg et al., 2010). Both strains of FHM1 mutant mice exhibit an enhanced excitatory, but apparently unchanged inhibitory, cortical neurotransmission (Vecchia et al., 2014; Vecchia et al., 2015) that can explain their increased susceptibility to experimentally induced CSD that is more pronounced with the S218L mutation (Van den Maagdenberg et al., 2004; Eikermann-Haerter et al., 2009; Tottene et al., 2009; Van den Maagdenberg et al., 2010). This seems in line with the more severe phenotype in patients carrying the S218L mutation, who can have epilepsy, cerebellar ataxia, and even can have fatal edema after only a mild head trauma, in addition to their prolonged hemiplegic attacks that are characterized by motor weakness (Kors et al., 2001; Chan et al., 2008; Stam et al., 2009). In contrast, carriers of the R192Q mutation have hemiplegic migraine without these additional clinical features (Ophoff et al., 1996). Here, we investigated heterozygous S218L mutant mice, who unlike the homozygotes do not have the additional features seen in patients with this mutation (Van den Maagdenberg et al., 2010) and compared these with homozygous R192Q mutant mice, to increase chances of finding spontaneous CSD events without the confounding of the additional features.

First, we investigated the occurrence and characteristics of (rare) spontaneous CSD events in freely behaving FHM1 mutant mice. Next, to compare features of spontaneous events with those of events induced in a controlled manner using optogenetics, we crossbred FHM1 mutant mice with transgenic mice that express light-sensitive channelrhodopsin-2 (ChR2) cation channels. Notably, we induce CSDs using optogenetics in mutant mice who also experience spontaneous CSD events, thus creating as it were superimposing attacks, which cannot be avoided when comparing the characteristics of both types of events. This approach is not different from what is done in humans where attacks are provoked by various agents in patients that also have spontaneous migraine attacks (Ashina et al., 2022). Also this approach allowed for activation of cortical neuronal networks and induction of CSD events by shining blue light through the intact skull in freely behaving mutant and wildtype mice to investigate the impact of CSD on cortical neuronal network activity and behaviour, also in relation to sleep. Our findings show rare spontaneous CSD events in FHM1 mutant mice, notably with key neurobiological and behavioural features also found in optogenetically induced events that make studies to understand the occurrence of such events feasible.

2. Materials and methods

2.1. Animals

Transgenic knock-in *Cacna1a*^{R192Q} and *Cacna1a*^{S218L} mice, harbouring missense mutations R192Q or S218L, respectively, were generated using a gene-targeting approach (Van den Maagdenberg et al., 2004; Van den Maagdenberg et al., 2010). For studying the spontaneous occurrence of CSD events, homozygous *Cacna1a*^{R192Q}, heterozygous *Cacna1a*^{S218L} mice, and wildtype (WT) littermates mice, 3 to 6 months of age, were used that had been backcrossed to C57BL/6J mice for at least 10 generations. For the optogenetics experiments, FHM1 mutant mice were crossbred with Thy1-ChR2-YFP mice (strain 7612 – B6.Cg-Tg (Thy1-COP4/EYFP)18Gfng/J; Thy1/ChR2-YFP, hemizygous line 18; $ChR^{+/-}$; the Jackson Laboratory) that express channelrhodopsin-2 in cortical neurons. All mice (WT and FHM1 mutants) used in the optogenetic experiments were homozygous for ChR2 (i.e., $ChR2^{+/+}$). Male mice were used for the experiments, unless mentioned otherwise. Mice were maintained under standard housing conditions with a 12-h light/dark cycle, with food and water ad libitum. Experimental interventions were carried out during the light period. Experiments were approved by local and national ethical committees in accordance with recommendations of the European Communities Council Directive (2010/63/EU) and were carried out in accordance with ARRIVE guidelines. All efforts were made to minimize suffering.

2.2. Detecting spontaneous CSD events in freely behaving FHM1 mutant mice

Surgery – Electrodes (single or paired 75 μm platinum (Pt)/iridium (Ir), PT6718; Advent Research Materials, Oxford, UK) were stereotaxically implanted under isoflurane anesthesia (induction 4%; maintenance 1.5% in oxygen-enriched air) at the following coordinates (mm to bregma): in the right hemisphere 1.0 anterior/1.5 lateral/0.7 depth (right motor cortex, M1; Pt/Ir); 3.5 posterior/2.0 lateral/0.4 depth (right visual cortex, V1; Pt/Ir); in the left hemisphere 1 Pt/Ir electrode was placed in either M1 or V1 at the same coordinates as for the right hemisphere. In case of neuronal multi-unit activity (MUA) recordings, paired electrodes were used. Two silver (Ag) ball-tip electrodes (75 μm, AG5493; Advent Research Materials) were placed above the cerebellum and served as reference and ground. Electrodes were connected to a 7-channel pedestal (E363/0 socket contacts and MS373 pedestal, Plastics One, Roanoke, VA, USA) and secured to the skull using dental cement (DiaDent Europe, Almere, the Netherlands). Carprofen (5 mg/kg, s.c.) was administered for post-operative pain relief.

Electrophysiological recordings – One week after surgery, electrocorticogram (ECoG) and synchronized video recordings were started in a shielded electrophysiological set-up for freely behaving mice, as previously described (Houben et al., 2017). Electrophysiological signals were 3× pre-amplified and fed into separate amplifiers for direct current (DC)-potential (500 Hz low-pass; 10× gain) and alternating current (AC)-potential (0.05–500 Hz; 800× gain), respectively. Signals were digitized (Power 1401 and Spike2 software, CED, Cambridge, UK) at a sampling rate of 1000 Hz (DC-potential) or 5000 Hz (AC-potential). Differential signals from paired cortical electrodes were used to detect neuronal MUA signals (500–5000 Hz; 36,000× amplification; 25,000 Hz sampling rate). MUA signals were processed offline for quantification of spike rate using Spike2 software. Behavioural activity was recorded on video (acA1300-60gmNIR camera, 30 frames/s, Basler, Ahrensburg, Germany) and with custom-built infrared locomotion and drinking sensors.

2.3. Optogenetically induced CSD in freely behaving mice

Surgery – Electrodes (single or paired 75 μm Pt/Ir) were implanted as described in section 2.2., but at the following coordinates (mm to

bregma): 3.0 posterior/2.0 lateral/0.6 depth (right V1); 1.0 anterior/2.0 lateral/0.8 depth (right M1); 3.0 posterior/2.0 lateral/0.6 depth (left V1); two Pt/Ir electrodes (with 1-mm uninsulated tips) in the cerebellum served as reference and ground. In a subset of mice, subcortical DC-potential recordings were obtained from Pt/Ir electrodes implanted at the following coordinates in left and/or right hemispheres: 0.5 anterior/2.0 lateral/3.0 depth (striatum); 1.8 posterior/1.2 lateral/1.2 depth (hippocampal CA1 region). Optic fiber cannulas (400 μm, Thorlabs, Newton, NJ, USA) for photo-stimulation were placed on the skull bone over the left and/or right M1 (1.5 mm anterior and 2.0 mm lateral to bregma) and left and/or right V1 (3.5 mm posterior and 2.0 mm lateral to bregma); locations were similar as for optogenetic CSD inductions in WT mice (Chung et al., 2019). Electrodes (connected to a 7-channel pedestal as described for the spontaneous recordings) and optic fibers were attached to the skull using dental cement (Simplex Rapid Powder; Kemdent, Swindon, UK) mixed with cyanoacrylate glue (KG385; Elmer's Products, Westerville, OH, USA). Carprofen (5 mg/kg, s.c.) was administered for post-operative pain relief.

Optogenetic photo-stimulation for induction of CSD and transcallosal evoked potentials – One week after surgery, mice were placed in the recording set-up and electrophysiological signals were acquired in freely behaving mice, as described for spontaneous CSD detection in section 2.2. Optogenetic stimulation experiments were started after 1 to 7 days of baseline ECoG and MUA recording. CSD threshold assessment was followed by additional optogenetics experiments described below, on separate days in random order, up to 1 month after surgery. A 460-nm LED light source (UHP-T-LED-460; Prizmatix, Givat-Shmuel, Israel) was connected to the optic fiber for blue light stimulation in the electrophysiology set-up (Houben et al., 2017). Delivered power at the optic cannula tip was calibrated to 4 mW before the experimental series (PM100A with S121C photodiode; Thorlabs). For assessing the CSD threshold, single 4-mW blue light pulses were applied to the right V1 at 5-min intervals with increasing pulse duration (in s: 0.01, 1, 2, 3, 4, 5, 6, 7, 8, 9, 10, 11, 12, 13, 14, 15, 16, 17, 18, 20, 30) and (on a different day) to the right M1 (in s: 0.3, 0.6, 0.9, 1.2, 1.5, 1.8, 2.1, 2.4, 2.7, 3, 4, 5, 6, 7, 8, 9, 10, 12, 15, 20, 30) until CSD was observed. If 4-mW pulses were unable to induce CSD, 30-s pulses with increasing intensity (up to 12 mW) were used. For comparison of CSD thresholds while mice were awake or in non-REM sleep, continuous blue light pulses were applied to the M1 cortex, once mice were in a certain vigilance state, until CSD occurred. This method was repeated on separate days with two days in-between recordings. Mice were randomly assigned to groups that started with CSD threshold recordings either during the awake or non-REM state. To assess effects of CSD on neuronal activity, as measured by changes in transcallosal evoked potential (TCEP) amplitude, TCEPs were recorded from the right M1 in response to optogenetic stimulation (at 0.1 Hz; 2-ms pulse duration) of the left M1 cortex. First, the half-maximal TCEP response amplitude was determined by increasing light intensity every 10 pulses, starting from 1.5 mW to a maximum of 22.5 mW. The stimulation intensity yielding a half-maximal response amplitude was used during a 1-h TCEP paradigm of 0.1-Hz single-pulse stimulation of the left M1, in combination with optogenetic CSD induction in the right V1 by a light pulse at threshold intensity with a duration of ~125% of the threshold duration, 10 min after the start of transcallosal stimulation. With the short photostimulations used for evoking TCEPs (with transcallosal stimulation of left M1, that is in the hemisphere contralateral to the right hemisphere in which CSD was induced in V1), no effects were observed on the propensity or shape of the CSD events induced in the right V1 for either WT or mutant mice.

2.4. Electrophysiological data analysis

Data were analysed off-line using Spike2 software and custom-written MATLAB® scripts (Mathworks, Natick, MA, USA). CSD was defined as a transient negative DC-shift with amplitude >5 mV measured with a delay at two recording locations and (in case of MUA recordings) accompanied by a depression of local MUA. For assessment of spontaneous CSD events, 7 days of recording were analysed starting 24 h after connecting the mouse to the electrophysiology set-up.

ECoG spectral power – Twenty four-h ECoG epochs were selected to be at least 24 h after the start of the recording (to avoid novelty or stress induced changes related to connection of the mouse to the set-up), not containing a spontaneous CSD, nor one in the 12 h prior to the selected 24-h epoch. V1 AC-ECoG signals were low-pass filtered at 100 Hz and down-sampled to 200 Hz. Power spectra were computed using a Fast Fourier Transform routine (Hanning window, 0.25-Hz resolution) per 4-s epoch. Total power was calculated for five defined spectral bands, i.e., delta (0.75–5 Hz), theta (5–10 Hz), alpha (10–15 Hz), beta (15–30 Hz), and gamma (30–45 Hz). Vigilance states (active waking, REM, and non-REM sleep) were determined by applying an automated algorithm based on recorded movements (assessed by the infra-red motion sensor, licking sensor, and video) and ECoG spectral composition. In the algorithm, epochs with locomotor or drinking activity were classified as active waking. The first 10 epochs following cessation of behavioural activity were classified as passive waking (Fisher et al., 2012) and were not used for spectral comparisons. Remaining epochs were classified as sleeping and further subdivided into REM (high-theta, i.e., > average theta power) and low-delta (< average delta power), and non-REM sleep (strong delta activity, i.e., > 2× average delta power) based on the V1 ECoG power spectrum. Sleep epochs not fulfilling the above criteria were left unclassified.

Vigilance state determined for the 10-min period prior to a spontaneous CSD event was assessed by visual inspection of V1 power spectra and analysis of behavioural activity assessed from video and the PIR movement sensor, categorized as active awake (high-theta and low-delta activity, during periods of movement), non-REM sleep (high-delta activity, no movements) or REM sleep (high-theta and low-delta activity following a period of non-REM sleep, no movements). For optogenetic CSD induction during active awake or non-REM sleep, this method of vigilance state detection was implemented real-time while monitoring mice in the recording cage. CSD was induced optogenetically when mice were actively awake or in non-REM sleep for a 5-min period.

Transcallosal evoked responses – M1 AC-ECoG recordings containing 0.1-Hz TCEPs in relation to optogenetic CSD were high-pass filtered at 0.1 Hz (3th order Butterworth, zero-phase shift). N1 peak amplitude and latency were detected between 3 and 15 ms after stimulation, and P1 peak amplitude and latency between the N1 peak latency and 40 ms. TCEP recovery following CSD was assessed by calculating N1-P1 amplitudes, normalized with respect to the averaged values prior to CSD from an individual mouse.

2.5. Behavioural analyses

Behaviour was analysed off-line using a software-based scoring system (The Observer 12.5; Noldus Information Technology, Wageningen, the Netherlands) starting 20 min before until 40 min after CSD. Start and end times of each type of behaviour were scored at 1-s precision. For the analysis, behaviours were grouped into active behaviour (e.g., walking, grooming, eating, scratching, stretching, being alert, exploratory activity) and inactive behaviour (e.g., sitting motionless, lying on the cage floor, sleeping). Total active behaviour was calculated for each 1-min bin from the summed duration of all types of behaviour, except inactivity.

Spontaneous behaviour of non-operated *Cacna1a*^{S218L} mice was analysed using video-tracking of animals placed in a Phenotyper® cage (Noldus Information Technology) equipped with a top view camera. Behaviour was tracked based on automatic detection of the body centre-point, nose-point, and tail-base (Ethovision XT 11.5; Noldus Information Technology) allowing for detection of general movements through the cage, body posture, and specific behaviours, including body stretching and head turning. Full body stretches were detected from the tracked data by setting the threshold for body elongation at 70% of the maximal

body length. Video inspection of behaviour was used for confirmation and to determine the complete behaviour before and after identified full body stretches.

2.6. Wire grip test

After optogenetically induced CSD, while still in the electrophysiological recording set-up, mice were lifted by the tail and allowed to grab onto a horizontal wire to assess grip performance, as described before (Houben et al., 2017). Lifting was repeated every 10 s, starting 1 min before CSD induction and lasting for 12 min. Videos were analysed by two observers (IL and MS) blinded for genotype; results were averaged. Successful wire grabbing was scored for both forepaws at 0.5-s precision to obtain a total grab duration over a 10-s bin. If a mouse grabbed the wire for a subset of the 0.5-s time window, this bin was scored under 'grabbing'. Simultaneously, recorded DC-potential and MUA were used to determine the time point of CSD reaching the M1 cortex.

2.7. Histology

After completion of the electrophysiological and behavioural experiments, mice were euthanized by CO_2 and transcardially perfused (0.1 M phosphate-buffered saline followed by 4% paraformaldehyde (PFA) in 0.1 M phosphate buffer). Brains were isolated, post-fixed in 4% PFA for 2.5 h at room temperature and sucrose-processed. Sagittal 40-μm sections were obtained with a freeze sliding microtome and Nissl-stained to verify electrode placement.

2.8. Statistical analysis

Data visualization and statistical testing were performed using Graphpad Prism (GraphPad Software). Data were presented as mean ± standard error of the mean (SEM) and analysed using 2-tailed paired or unpaired *t*-tests, Kruskal-Wallis test, repeated measures one-way or two-way ANOVA, or mixed-effects analysis, as appropriate. A p-value <0.05 was considered significant.

3. Results

3.1. Rare spontaneous CSD events in FHM1 mutant mice

During a period of 7 days of continuous ECoG and neuronal activity recording following 1 week recovery from surgery, rare spontaneous CSD events were detected in freely behaving FHM1 mutant mice, but never in WT mice ($n = 10$ per genotype): four events were observed in 3 out of 10 recorded *Cacna1a*^{R192Q} mice and two events in 2 out of 10 recorded *Cacna1a*^{S218L} mice (example traces in Fig. 1A, B). CSDs in all three *Cacna1a*^{R192Q} mice consisted of a single CSD wave, whereas in the two *Cacna1a*^{S218L} mice multiple consecutive CSD waves were observed per event (1 animal showing 2 waves, 1 animal showing 3 waves). All CSDs were characterized by a pronounced DC-potential shift that coincided with a peak in neuronal MUA, followed by suppression of cortical neuronal activity. The mean CSD amplitude was 12.5 ± 4.3 mV for the four events in *Cacna1a*^{R192Q} mice and 12.8 and 16.4 mV, respectively, for the two events in *Cacna1a*^{S218L} mice, with a mean half-width of 49.5 ± 11.1 s in *Cacna1a*^{R192Q} mice and 41.1 and 50.5 s for the events in *Cacna1a*^{S218L} mice (analysed at the electrode location where CSD was first detected). The right hemisphere provided information on the path that CSD followed in the cortex, as it contained electrodes in both M1 and V1. For one event in *Cacna1a*^{R192Q} mice and for both events in *Cacna1a*^{S218L} mice, CSDs were first observed in V1 and subsequently in M1 cortex. CSDs in the other two *Cacna1a*^{R192Q} mice were first detected in M1 or near-simultaneously in right M1 and V1 cortex, suggesting an origin with similar proximity to the V1 and M1 electrodes in the latter. In the left hemisphere, that contained a single electrode, a contralateral CSD wave was observed for all events in the *Cacna1a*^{R192Q} mice, but not for the events in *Cacna1a*^{S218L} mice.

3.2. FHM1 mutant mice display enhanced ECoG gamma activity indicative of cortical hyperexcitability

To assess whether changes in cortical network activity may underlie the susceptibility to spontaneous CSD events, we compared the spectral composition of ECoG from V1 cortex for *Cacna1a*^{R192Q}, *Cacna1a*^{S218L}, and WT mice. ECoG power was calculated for a 24-h period (without a

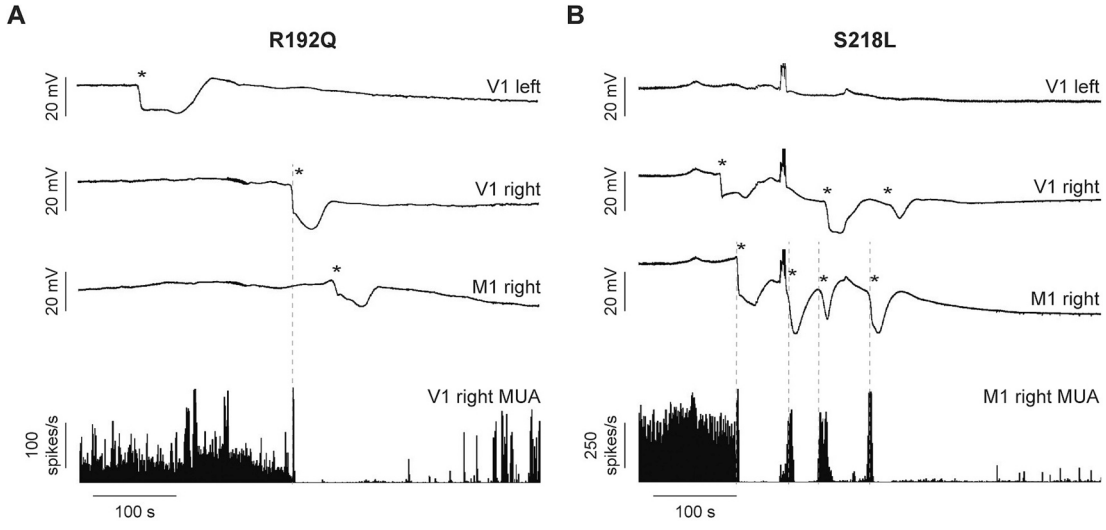

Fig. 1. Neurophysiological characteristics of spontaneous CSD events occasionally observed in freely behaving FHM1 mutant mice. Example DC-potential and MUA traces of spontaneously occurring CSD events (* indicating the >5 mV negative DC-potential shift reflecting a single wave) recorded in a subset of *Cacna1a*^{R192Q} (A) and a *Cacna1a*^{S218L} (B) mice. CSD waves were associated with an initial peak in cortical MUA, followed by MUA suppression indicating inhibition of neuronal activity. Dotted lines indicate the MUA peak coinciding with the start of the corresponding DC-shift at the same cortical location. Note that in the example of the *Cacna1a*^{R192Q} mouse, the CSD was first detected in the left hemisphere, followed by detection in the right hemisphere. In the *Cacna1a*^{S218L} mouse, the CSD consisted of multiple waves, similar as in the other *Cacna1a*^{S218L} mouse in which spontaneous events were observed, while spontaneous events in *Cacna1a*^{R192Q} always consisted of a single CSD wave.

CSD event) across vigilance states, i,e., separated for active waking, REM, and non-REM sleep (Fig. 2A). As a divergence in power was observed towards the higher end of the frequency spectrum, spectral power in the gamma (γ, 30–45 Hz) frequency band was compared across genotypes and found to be higher in *Cacna1a*^{R192Q} compared to WT mice across all vigilance states ($p < 0.001$ for active waking and non-REM and $p = 0.016$ for REM sleep). In *Cacna1a*^{S218L} mice, only a mild increase in γ-band power was observed during active waking compared to WT ($p = 0.026$) and not for the other vigilance states. The enhancement of γ-band power did not cluster with respect to the mice displaying spontaneous CSD events. Compared to *Cacna1a*^{R192Q} mice, γ-band power was lower in *Cacna1a*^{S218L} for active waking ($p < 0.001$) and REM sleep ($p = 0.002$; Fig. 2B). Vigilance state distribution in the 24-h periods did not differ between *Cacna1a*^{R192Q} and WT mice, while *Cacna1a*^{S218L} mice displayed reduced periods of active waking and increased periods of REM sleep in comparison to WT mice ($p = 0.0005$ for waking, $p < 0.0001$ for REM) and slightly reduced periods of active waking and increased periods of REM sleep in comparison to *Cacna1a*^{R192Q} mice ($p = 0.047$ and p < 0.0001, respectively).

3.3. FHM1 mutant mice show enhanced susceptibility to optogenetically induced CSD

Given the rare occurrence of spontaneous CSD events in FHM1 mutant mice, which makes their investigation not practical, we next performed optogenetic photo-stimulation over the intact skull to induce CSD in a controlled minimally invasive manner (schematic representation in Fig. 3A). Thus, we characterized in detail CSD features in freely behaving *Cacna1a*^{R192Q}, *Cacna1a*^{S218L} and WT mice that also expressed channelrhodopsin-2 in cortical neurons. CSD could be reliably induced in all genotypes by providing blue light pulses of increasing intensity (range: 4–12 mW) and duration (range: 1–30 s) over the right V1 cortex.

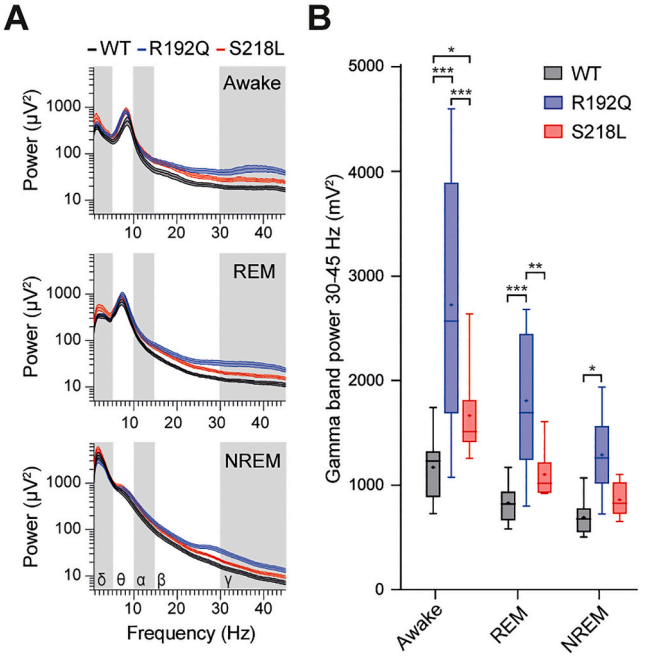

Fig. 2. Enhanced ECoG γ-band power in CSD-free periods in freely behaving FHM1 mutant transgenic mice. (A) Averaged power spectra (1–45 Hz) of V1 cortex ECoG during active waking (top), REM sleep (middle), and non-REM sleep (bottom) in WT ($n = 10$), *Cacna1a*^{R192Q} (n = 10) and *Cacna1a*^{S218L} (n = 10) mice. (B) *Cacna1a*^{R192Q} and *Cacna1a*^{S218L} mice displayed enhanced power in the lower γ-band (30–45 Hz) compared to WT (p < 0.001). Whiskers show minimum-to-maximum values, + sign indicates the mean. * corrected $p <$ 0.05, ** corrected $p < 0.01$, *** corrected p < 0.001 (false discovery rate corrected multiple comparisons test).

Following optogenetic stimulation, all CSD events in *Cacna1a*^{R192Q} mice (6 males, 6 females) and WT mice (8 males, 6 females) consisted of a single wave (example trace from a *Cacna1a*^{R192Q} mouse in Fig. 3B). Multiple-wave CSD events were recorded in all but one *Cacna1a*^{S218L} mice (6 males, 5 females; example trace in Fig. 3C) for the first optogenetically induced CSD. For optogenetically induced CSD events on later days, *Cacna1a*^{S218L} mice showed both single- and multiple-wave events, with the % of multiple-wave events ranging from about 30–40%. Of note, induced CSD events did not spread to the contralateral hemisphere in any of the genotypes. CSD propagation speed, measured between the right V1 and M1 location, was faster in both *Cacna1a*^{R192Q} and *Cacna1a*^{S218L} mice compared to WT ($p = 0.003$ and $p < 0.0001$, respectively; Fig. 3D). CSD propagation speed was higher in females compared to males for *Cacna1a*^{S218L} mice ($p = 0.001$), whereas no sex difference was noted for *Cacna1a*^{R192Q} and WT mice (*p*-values of 0.13 and 0.23, respectively; Fig. 3D). CSD amplitude and half-width duration (assessed from the M1 CSD event) were not different across genotypes (amplitude: $p > 0.99$ for WT vs. *Cacna1a*^{R192Q} and *Cacna1a*^{S218L}, $p =$ 0.51 for *Cacna1a*^{R192Q} and *Cacna1a*^{S218L}, half-width duration: p > 0.99 for comparison of all genotypes). Hence, for further optogenetic experimentation, only male mice were used.

To compare the threshold for CSD initiation across genotypes, 4-mW pulses with increasing pulse durations were first applied to V1 cortex, but as described before (Chung et al., 2019), thresholds in V1 were variable. CSD could be induced in V1 using a 4-mW power only in a subset of mice, i.e., in 4 out of 7 WT, 6 out of 8 *Cacna1a*^{R192Q}, and 5 out of 7 *Cacna1a*^{S218L} mice, with a threshold pulse duration ranging from 6 to 8 s in WT, 3–8 s in *Cacna1a*^{R192Q} and 3–13 s in *Cacna1a*^{S218L} mice (Fig. 3E). However, with photo-stimulation in M1 cortex, again as shown earlier (Chung et al., 2019), the threshold was less variable and lower, yielding a 100% success rate when stimulating with 4 mW for all genotypes. The M1 CSD threshold pulse duration was lower for *Cacna1a*^{R192Q} and *Cacna1a*^{S218L} mice compared to WT mice (*p*-values 0,044 and 0.008, respectively; Fig. 3E).

Next, we assessed whether the CSD induction threshold in FHM1 mutant mice remained stable over time, as we had demonstrated over a 1-week period in WT animals (Houben et al., 2017). To this end, CSD was repeatedly induced via photo-stimulation of the M1 cortex in *Cacna1a*^{S218L} ($n = 4$) and WT mice ($n = 6$), two times per week over a period of about three weeks (i.e., 23 days), starting 1 week (i.e., 7 days) after surgery. For all time points, *Cacna1a*^{S218L} mice showed a lower CSD induction threshold and higher CSD propagation speed compared to WT mice (all below $p < 0.05$; Fig. 3F). CSD induction threshold and propagation speed appeared stable over time for both *Cacna1a*^{S218L} and WT mice, with induction threshold and propagation speed at 30 days not differing from those at day 7 after surgery (WT: p-values 0.35 and > 0.99, respectively; for *Cacna1a*^{S218L}: p-values 0.74 and 0.2, respectively).

3.4. Recovery of cortical activity following optogenetically induced CSD

Previously, optogenetically induced CSD was found to strongly suppress cortical neuronal activity for at least 40 min in freely behaving WT mice (Houben et al., 2017). To assess whether the presence of an FHM1 mutation influences cortical recovery after CSD, cortical MUA following optogenetically induced CSD was compared between *Cacna1a*^{S218L} and WT mice. After V1 CSD induction, in both genotypes, M1 cortical neuronal MUA levels were strongly suppressed in the 20-min period following the start of the detected CSD in M1, to a level of 32 ± 11% in WT and 30 ± 12% in *Cacna1a*^{S218L} mice with respect to MUA levels in the 20-min period preceding CSD ($n = 5$ per group; example traces in Fig. 4A). Cortical MUA was still not fully recovered within 1 h following CSD, but recovery was faster in *Cacna1a*^{S218L} than WT mice: in the 40- to 60-min window post-CSD, *Cacna1a*^{S218L} mice showed 81 ± 6% recovery of cortical MUA, compared to 50 ± 17% in WT mice (Fig. 4B; $p = 0.029$).

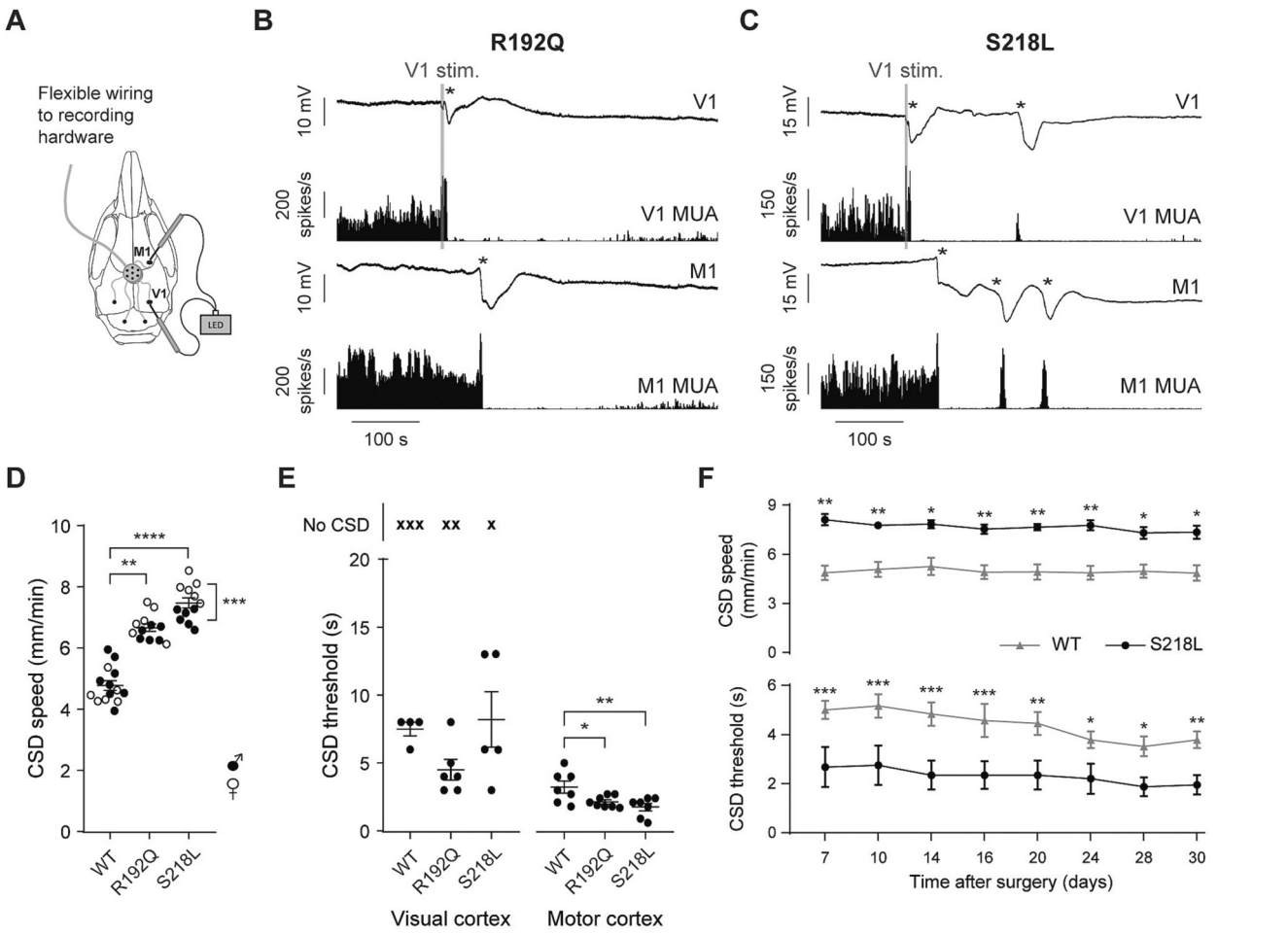

Fig. 3. Optogenetic CSD characteristics in FHM1 mutant and WT mice. (A) Schematic representation of recording electrode and optic fiber stimulation locations. Example DC-potential and MUA traces of CSD induced by optogenetic photo-stimulation of the right V1 cortex, recorded in a *Cacna1a*^{R192Q} (B) and a *Cacna1a*^{S218L} (C) mouse. Note that in the *Cacna1a*^{S218L} mouse, as observed for the cases of spontaneously occurring CSDs, the CSD consisted of multiple waves (asterisks indicating individual CSD waves). Each start of the CSD wave was associated with a peak in cortical MUA followed by a reduction indicating suppression of neuronal activity. (D) CSD propagation speed was increased in FHM1 mutant compared to WT mice (Kruskal-Wallis test correcting for multiple comparisons), with *Cacna1a*^{S218L} mice showing a higher propagation rate in females compared to males (unpaired *t*-test; WT: $n = 8$ males, 6 females; *Cacna1a*^{R192Q}: $n = 6$ males, 6 females; *Cacna1a*^{S218L} mice: n = 6 males, 6 females). (E) Photo-stimulation with 4-mW blue light pulses on the V1 cortex evoked CSD in all cases for *Cacna1a* mutant ($n = 7$ *Cacna1a*^{R192Q}, n = 7 *Cacna1a*^{S218L}) but not in WT mice (n = 7) while photo-stimulation of the M1 cortex in the same mice resulted in a 100% success rate in all genotypes while revealing lower threshold pulse durations for CSD induction in FHM1 mutant mice (one-way ANOVA correcting for multiple comparisons). (F) Repeated optogenetic CSD induction at 2- to 4-days interval shows stable CSD propagation rates over the course of the 23-day period, with *Cacna1a*^{S218L} mice showing higher CSD propagation rates at all time points (two-way ANOVA correcting for multiple comparisons). Optogenetic CSD induction thresholds showed a slight but non-significant reduction towards the end of the 30-day testing period for both mutant *Cacna1a*^{S218L} ($n = 4$) and WT (n = 6) mice (two-way ANOVA correcting for multiple comparisons). At all time points, *Cacna1a*^{S218L} mice showed lower CSD induction thresholds (two-way ANOVA correcting for multiple comparisons). *$p < 0.05$; **$p < 0.01$; ***$p < 0.001$; ****$p < 0.0001$.

Additionally, we determined cortical neuronal MUA recovery following the few spontaneous CSD events that were observed in *Cacna1a*^{R192Q} and *Cacna1a*^{S218L} mice. In the 40- to 60-min-period following the start of CSD, cortical MUA in the two *Cacna1a*^{S218L} mice recovered to 64% and 92% of pre-CSD levels, whereas for the four CSD events in three *Cacna1a*^{R192Q} mice recovery was only 48 ± 10%, suggesting a, perhaps unexpected, faster MUA recovery for the more severely affected *Cacna1a*^{S218L} mice. The rare occurrence of spontaneous CSDs did not allow a genotypic difference in recovery to be statistically tested.

Next, we determined recovery of evoked cortical network activity following CSD by recording transcallosal evoked responses (TCEPs) in the right M1 cortex (i.e., the hemisphere in which CSD was induced). For this, TCEPs were evoked by 0.1-Hz transcallosal stimulation of the left M1 cortex (i.e., the hemisphere contralateral to the hemisphere in which CSD was induced in the V1 cortex) while local field potential and MUA were recorded in the right M1 cortex before, during and after optogenetic CSD induction in the right V1 cortex (Fig. 4C). TCEP features were compared between WT ($n = 7$) and *Cacna1a*^{S218L} mice, subdivided for *Cacna1a*^{S218L} mice displaying single-wave (n = 7) and multiple-wave ($n = 3$) CSD events. Cortical recovery was determined from TCEP N1-P1 amplitude changes following CSD. Fig. 4C shows example traces of TCEP and the corresponding DC-potential recordings for a single- and multiple-wave CSD in two *Cacna1a*^{S218L} mice. TCEP recovery did not differ between WT and *Cacna1a*^{S218L} mice with single-wave CSDs. Multiple-wave CSDs in *Cacna1a*^{S218L} mice, however, were associated with a longer TCEP recovery when compared to WT and *Cacna1a*^{S218L} mice with single-wave CSDs, as evident from the 3rd min following the start of CSD in M1 where TCEP amplitude only recovered to 39 ± 4% vs 73 ± 8% and 77 ± 8% in WT and *Cacna1a*^{S218L} mice with single-wave CSD, respectively (Fig. 4D; *p*-values 0.014 and 0.009, respectively). Notably, a full recovery of TCEP amplitude following single- and multiple-wave CSDs was observed within 5 min following CSD initiation, which was faster than the recovery of MUA, which did not even recover in the 60 min following CSD.

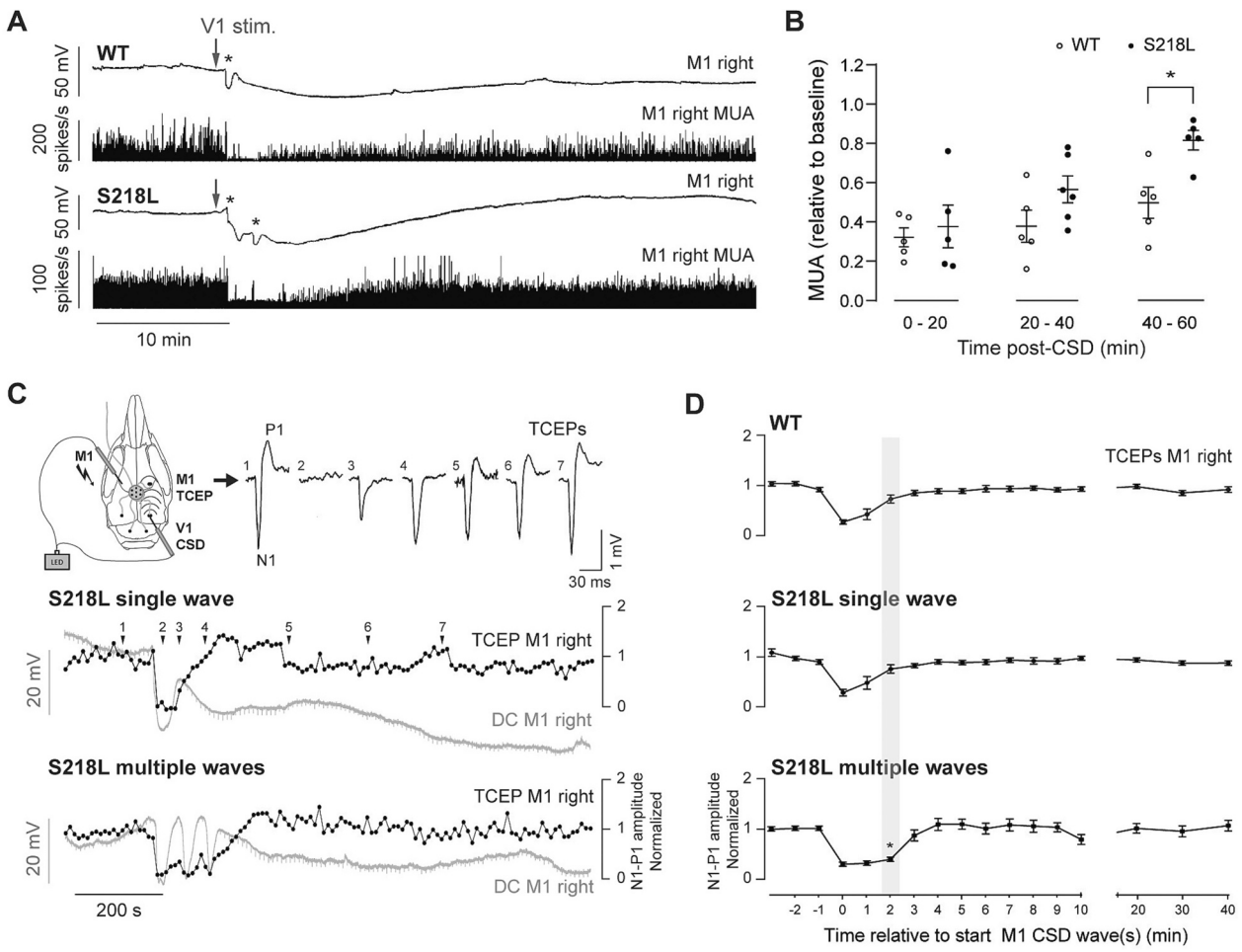

Fig. 4. Post-CSD recovery of cortical neuronal multi-unit activity (MUA) and transcallosal evoked potentials in WT and *Cacna1a*^{S218L} mice. (A) Example DC-potential and MUA traces of WT and *Cacna1a*^{S218L} mice showing suppression and recovery of neuronal activity following optogenetic CSD induced by V1 photo-stimulation (asterisks indicating individual M1 CSD waves). Note that the CSD event in the *Cacna1a*^{S218L} mice consisted of a dual wave. (B) *Cacna1a*^{S218L} mice (that all displayed multiple wave CSDs in the experiments) showed faster recovery of neuronal activity following optogenetic CSD, as reflected by higher MUA levels in the 40–60-min period after CSD compared to WT mice (two-way ANOVA correcting for multiple comparisons; $n = 5$ per genotype). (C) Left: schematic representation of the transcallosal stimulation paradigm combined with V1 optogenetic CSD induction. Transcallosal evoked potentials (TCEP) were obtained by 0.1-Hz transcallosal stimulation using an optic fiber placed on the left M1 cortex, while recording DC- and field-potentials in the right M1 cortex. CSD was optogenetically induced in the right V1 cortex 10 min after start of transcallosal stimulation. Example traces of TCEP values (normalized to the averaged pre-CSD amplitude) and DC-potential are shown from two *Cacna1a*^{S218L} mice with, respectively, a single- and multiple-wave CSD. Individual TCEP responses shown at the right top correspond to the numbered arrows in the single CSD example, showing recovery of N1-P1 amplitude within 2 min following optogenetic CSD in M1. N1–P1 TCEP values and DC-potential overlays indicate that multiple wave CSDs are associated with a longer TCEP recovery period. (D) Relative TCEP N1–P1 amplitudes averaged for WT, *Cacna1a*^{S218L} with a single-wave CSD, and *Cacna1a*^{S218L} with multiple-wave CSDs ($n = 7$, $n = 7$, and $n = 3$, respectively), plotted in 1-min time bins, show that TCEP recovery takes longer following multiple-wave CSDs, as evident from a significantly more reduced N1–P1 amplitude in the 2-min window following the start of M1 CSD (two-way ANOVA correcting for multiple comparisons). *$p < 0.05$.

3.5. Multiple-wave CSDs in *Cacna1a*^{S218L} mice are associated with a prolonged recovery of motor grip function

In WT mice, optogenetic CSD had previously been shown to impair contralateral motor function, as assessed by wire grip testing, between 30 and 300 s following CSD reaching the M1 cortex (Houben et al., 2017). Using the same approach, upon CSD induction in the right V1 cortex, we compared the impact of optogenetic CSD on motor function between FHM1 mutant and WT mice. Relative grab durations for the left and right forepaw were assessed over a period of 7.5 min starting after the end of the last CSD wave reaching the right M1 cortex, yielding a measure of motor impairment from the difference in grab duration of the left and right forepaw. Following CSD in the right hemisphere, mice of all genotypes showed impairment of left forepaw grip function compared to the right side (Fig. 5A), lasting up to 3 min after a single-wave CSD in WT mice ($n = 6$), *Cacna1a*^{R192Q} (n = 6) and *Cacna1a*^{S218L} ($n = 4$) mice (one-way ANOVA, correcting for multiple comparisons). *Cacna1a*^{S218L} mice with multiple-wave CSD events ($n = 3$) showed a significantly longer recovery time of the left forepaw's grab duration compared to both WT and *Cacna1a*^{R192Q} mice, which only had single-wave CSDs (Fig. 5B; all p-values <0.05 for the period between 4 and 6 min following the end of the last CSD wave reaching M1 cortex), and to single-wave CSDs in *Cacna1a*^{S218L} mice ($p = 0.008$, for the period between 5 and 6 min following the end of the last CSD wave reaching M1 cortex; two-way ANOVA correcting for multiple comparisons).

3.6. Optogenetically induced CSDs in FHM1 mutant mice are accompanied by specific behaviour

Behavioural characteristics associated with optogenetic CSD events in *Cacna1a*^{R192Q} (n = 5), *Cacna1a*^{S218L} (n = 6) and WT mice (n = 5) were determined from locomotor activity and video recordings. In all mice,

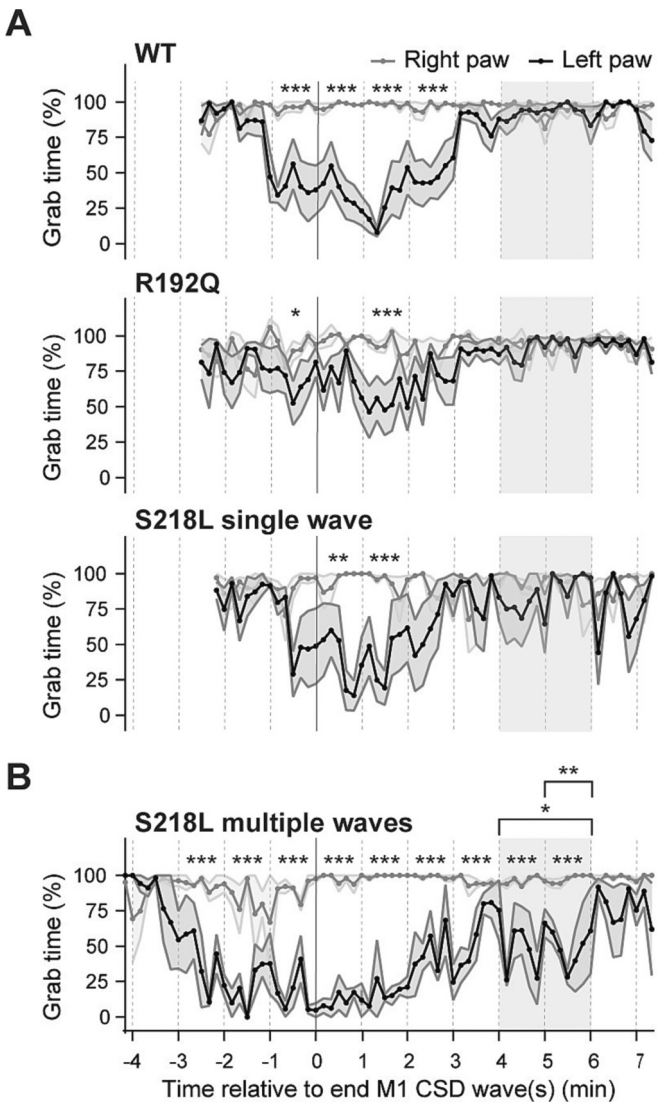

Fig. 5. Multiple-wave CSDs in *Cacna1a*^{S218L} mice are associated with a prolonged motor function impairment. Grab duration of the left and right forepaw, as assessed by wire grip testing, in relation to the end of a single CSD wave detected in the right M1 cortex (A) in WT ($n = 5$), *Cacna1a*^{R192Q} (n = 5), and *Cacna1a*^{S218L} mice (n = 4) or multiple-wave CSD (B) in *Cacna1a*^{S218L} mice (n = 3), shows transient impairment of left forepaw motor function following CSD, that is more pronounced for *Cacna1a*^{S218L} mice with multiple-wave CSD events. Grey area in the graphs indicating the time period in which more pronounced impairment of left forepaw grab duration is observed in *Cacna1a*^{S218L} mice with multiple wave CSDs. For the comparison to the single-wave events in WT and *Cacna1a*^{R192Q} mice this concerned the time period between 4 and 6 min following the end of CSD, and for the comparison to *Cacna1a*^{S218L} mice with a single wave CSD the period between 5 and 6 min. *$p < 0.05$; **$p < 0.01$; ***$p < 0.001$; ****$p < 0.0001$.

CSD (induced at threshold pulse duration with 4 mW in V1) led to an initial short increase in locomotor activity in the first 1–3 min following detection of CSD in M1, followed by a period of inactivity that could last up to 15 min before mice started moving again (Fig. 6A), as observed before in WT mice (Houben et al., 2017). *Cacna1a*^{S218L} mice started becoming active sooner (from about 10 min) after CSD compared to *Cacna1a*^{R192Q} mice ($p = 0.016$), whereas the period of inactivity was not different between *Cacna1a*^{R192Q} and WT animals ($p = 1.0$) in which locomotor activity returned to normal after ~15 min following CSD.

Detailed analyses of video data from optogenetic CSD events in these mice revealed the occurrence of three types of CSD-associated behaviour that were observed within the 2-min period surrounding arrival of a CSD event in the M1 cortex. Of these, full body stretches and head turning were observed with all genotypes (Fig. 6B), whereas one-directional rotating body movements were only observed in FHM1 mutant mice (in 4 out of 5 *Cacna1a*^{R192Q} and 5 out of 6 *Cacna1a*^{S218L} mice; see example in Supplementary Video 1). A combination of the behavioural features was seen in 3 out of 5 WT mice, 4 out of 5 *Cacna1a*^{R192Q}, and 5 out of 6 *Cacna1a*^{S218L} mice (Fig. 6B). One *Cacna1a*^{R192Q} and one *Cacna1a*^{S218L} mouse kept their head in a turned position for a prolonged period that could last up to 20 min following CSD. Such behaviour was not observed in WT mice.

The fact that rotating body movements were only seen in FHM1 mutant mice may suggest the involvement of subcortical SD, as described previously for these mice (Eikermann-Haerter et al., 2009; Eikermann-Haerter et al., 2011). We therefore assessed the occurrence of rotating body movements in more detail in *Cacna1a*^{S218L} and WT mice by placing additional recording electrodes in the striatum (caudate putamen region; $n = 6$ per genotype) and, in a subset, also in the hippocampus (CA1 region; $n = 4$ per genotype) to determine whether the CSD-related rotating body movements in mutants correlated to SD occurrence in subcortical brain structures. CSDs induced in the left or right V1 cortex were always associated with unilateral rotating body movements in *Cacna1a*^{S218L} mice, directed contralaterally to the side of CSD induction (Fig. 6C and D and see Supplementary Video 2). The far majority of CSD events in both the WT (11/12 events) and *Cacna1a*^{S218L} (11/12 events) mice was followed by SD in the striatum (example in Fig. 6C showing SD spreading through the striatum). All *Cacna1a*^{S218L} mice with a hippocampal electrode showed SD events in this region (example in Fig. 6D), whereas a hippocampal SD was never observed in WT mice. With respect to the time delay between the cortical and subcortical SDs in *Cacna1a*^{S218L} mice, striatal SD was observed 42.1 ± 17.3 s after SD detection in M1, followed by hippocampal SD observed 72.7 ± 26.7 s after SD detection in M1. Based on timing, rotating body movements were observed shortly before SDs reached the electrode in the striatum (2.2–0.5 s prior to the start of striatal SD).

3.7. Spontaneous CSD shows similar behaviour as optogenetically induced CSD

Considering the behavioural features observed with FHM1 mutant mice following optogenetically induced CSD, we next assessed CSD-related behaviour from video for the six spontaneous CSD events in *Cacna1a*^{R192Q} and *Cacna1a*^{S218L} mice for a 1-h period starting 20 min prior to until 40 min after CSD. The spontaneous CSD events were associated with one or more of the three behaviours, i.e., full body stretches, head turning and unilateral rotating body movements, seen with optogenetically induced CSD. The behaviours started in the period between 1 min prior to 1 min after the first detected CSD wave, lasted up to maximally 4 min following that wave, and were not present during the remaining observed time period (see example in Supplementary Video 3). Full body stretches were observed for all except one of the spontaneous CSD events, occurring immediately prior to or during the detected CSD wave. Within the 1-h observation period these stretches only occurred within the minutes surrounding the CSD event. Slow head turning movements were observed for 5 out of 6 CSD events, which often continued into an very pronounced turned head position of ~90 degrees that could persist for minutes. In 4 out of the 6 CSD events the initial head turning was followed by a unilateral rotating body movement resembling 'circling'. All except one CSD event were accompanied by a combination of the three mentioned CSD-associated behaviours: stretching, head turning, and rotating body movements were observed with three CSD events; the combination of only stretching and head turning was observed with one event; head turning combined with a rotating body movement was also observed with one event. Previously reported CSD-associated behaviours, such as freezing (Tepe et al., 2015) and wet-dog shakes (Akcali et al., 2010), were not observed.

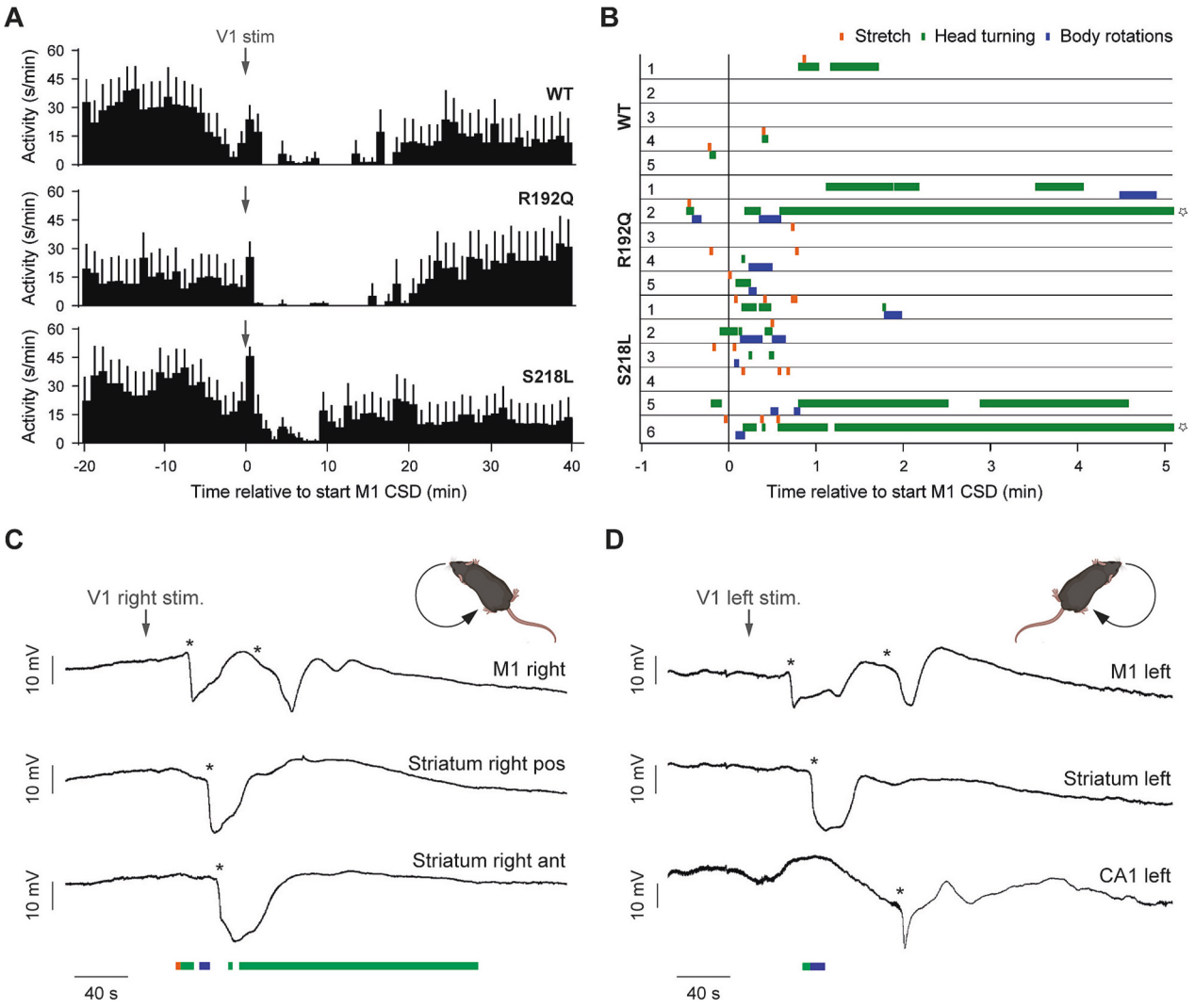

Fig. 6. Behavioural characteristics of optogenetically induced CSD in FHM1 mutant and WT mice. (A) Locomotor activity surrounding optogenetic CSD (induced here by V1 photo-stimulation), averaged for WT ($n = 5$), *Cacna1a*^{R192Q} (n = 5), and *Cacna1a*^{S218L} (n = 6) mice, depicted as active s per min. In WT and *Cacna1a*^{R192Q} mice, locomotor activity was reduced for a ~ 15-min period following CSD whereas in *Cacna1a*^{S218L} mice active behaviour returned after ~10 min. (B) Optogenetically induced CSD was associated with specific behaviours, i.e., full body stretches, slow one-directional head turning, and rotating body movements in the period surrounding CSD (1 min prior and 5 min following the detected CSD in M1) for the different mice tested for each genotype (indicated by numbers 1–5 or 1–6). Rotating body movements were only observed in FHM1 mutant mice (see also Supplementary Video 1 showing an example of CSD-associated behaviour for another CSD event, evoked on a different day by M1 stimulation in one of the *Cacna1a*^{S218L} mice). In some FHM1 mutant mice, head turning was observed as long as up to 20 min following CSD (indicated by open star symbols on the right site of the plot for the 2nd *Cacna1a*^{R192Q} mouse and the 6th *Cacna1a*^{S218L} mouse). Stretches and rotating body movements were observed in the 1-min pre-CSD to 5-min post-CSD period. (C) Example DC-potential traces of a *Cacna1a*^{S218L} mouse with subcortical electrodes in two striatal locations showing that SD propagated through the striatum (asterisks indicate individual SD waves), accompanied by SD-related behaviours (indicated below traces, in colours matching those of panel B) stretching, slow head turning, and rotating body movements contralateral to the side of stimulation. (D) Example DC-potential traces of a *Cacna1a*^{S218L} mouse showing that SD propagated from cortex to striatum and hippocampus, accompanied by head turning and rotating body movements contralateral to the side of stimulation.

In an attempt to assess the possible occurrence of a spontaneous CSD in unoperated, naïve, mice, solely based on behavioural tracking, video-recordings of *Cacna1a*^{S218L} mice ($n = 7$) were scored for the occurrence of full body stretches, slow head turning, and/or unilateral rotating body movements, as indication for a spontaneous CSD event. In the first full daylight period (6 a.m. - 6 p.m.) after placement of the mouse in the Phenotyper® home cage, in total 80 full body stretches were observed with a range of 4 to 16 per mouse. Subsequently, all stretching events were visually inspected for co-occurrence of slow head turning or unilateral body movement rotations, from 3 min before up to 3 min after the full body stretch. Only 1 out of 80 full body stretches was preceded by unilateral body rotation with slow head turning after the full body stretch. Hence a combination of the three behaviours within a limited time frame may possibly reflect a spontaneous CSD in a naive mouse, but the claim, as no electrodes are present, cannot be further substantiated.

3.8. CSD susceptibility is higher during non-REM sleep compared to waking

Spontaneous CSDs are associated with a peak in active behaviour starting either within the 1-min period before CSD or immediately following the start of CSD (Fig. 7A). Notably, all spontaneous CSDs were observed during the day, i.e., in the light period. To assess whether mice were awake or asleep prior to CSD, vigilance states were determined in the 10 min prior to CSD onset. In this period, all mice were predominantly in non-REM sleep (77 ± 2% of the 10-min period) intervened with short periods of waking (17 ± 2%) and/or REM sleep (6 ± 1%) (Fig. 7B). For 2 events, only non-REM and waking were observed.

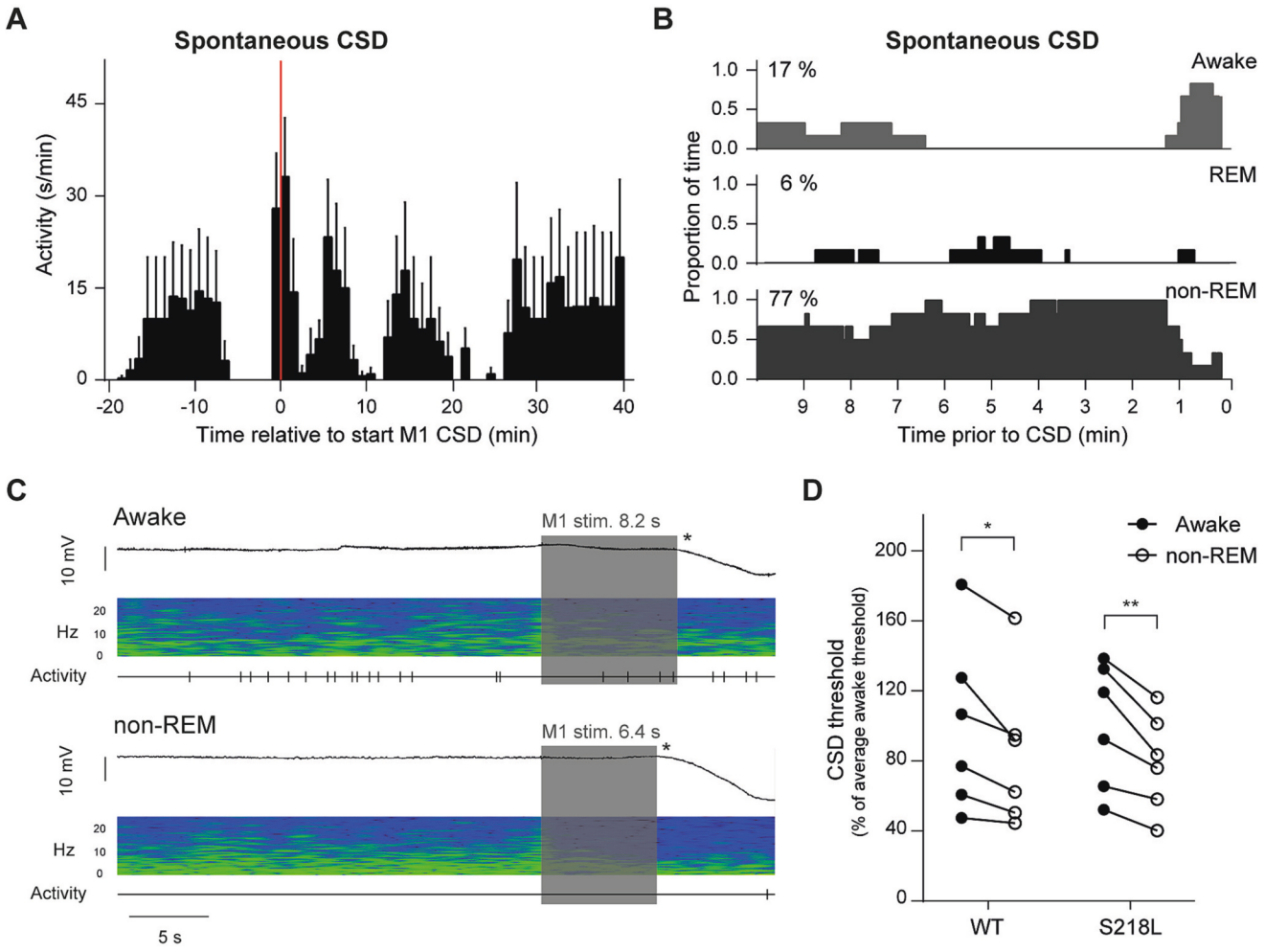

Fig. 7. Enhanced CSD susceptibility during non-REM sleep. (A) Directly before or after spontaneous CSD events observed in a subset of *Cacna1a*^{R192Q} and *Cacna1a*^{S218L} mice (n = 6 events), mice showed a peak in locomotor activity, preceded by a period of inactive behaviour. (B) Vigilance state distribution in the 10-min period preceding spontaneous CSD events. During the 10-min period preceding a spontaneous CSD event, *Cacna1a*^{R192Q} and *Cacna1a*^{S218L} mice were predominantly (77% of the time) in non-REM sleep. Shortly before CSD was first detected, in all except one case the animal woke up. (C) Example traces showing M1 photostimulation for optogenetic CSD induction (asterisk indicates individual CSD wave) in a WT mouse that was awake (upper panel) and, on a different day, in non-REM sleep (lower panel) for at least 5 min prior to stimulation. Continuous light stimulation was given until CSD was observed. (D) Graph showing threshold photo-stimulation pulse duration for optogenetic CSD induction in WT (n = 6) and *Cacna1a*^{S218L} mice (n = 6) during waking and non-REM sleep in individual mice. CSD threshold pulse durations are indicated as % of the average threshold obtained during the awake state, for WT and *Cacna1a*^{S218L} mice. For both genotypes, the threshold for inducing a CSD by optogenetics was lower during non-REM sleep than during waking (Paired *t*-test; $*p < 0.05$; $**p < 0.01$), with no genotypic differences for the threshold ratio between the non-REM and awake state.

Notably, in all cases, except for one CSD event in a *Cacna1a*^{R192Q} mouse, animals woke up shortly (56–87 s) before the first detected CSD wave.

To assess whether CSD susceptibility may be enhanced during non-REM sleep, as indicated for sleep vs waking by a recent study also using optogenetics in mice (Yousef Yengej et al., 2022), the M1 threshold for optogenetic CSD was assessed either during the active awake state or when mice were in non-REM sleep (in random order, with optogenetic stimulation within the same animal performed on a different day). Starting 3 min after the detected initiation of non-REM sleep or active waking, 4-mW blue light pulses to the M1 cortex were given continuously in WT ($n = 6$) and *Cacna1a*^{S218L} (n = 6), until CSD was detected (example traces from a WT mouse in Fig. 7C). This approach revealed a higher CSD susceptibility, indicated by a shorter light pulse duration required for CSD induction – thus lower CSD threshold – in non-REM sleep compared to the awake state. The optogenetic CSD threshold in non-REM sleep was reduced to 80 ± 7% of the threshold level during waking in WT and to 85 ± 8% in *Cacna1a*^{S218L} mice (Fig. 7D; $p = 0.017$ and $p = 0.006$, respectively), with no genotypic differences for the threshold ratio between the non-REM and awake state.

4. Discussion

Here we investigated neurophysiological and behavioural features of spontaneous CSD events in FHM1 mutant *Cacna1a*^{R192Q} and *Cacna1a*^{S218L} mice. In addition, we compared features of spontaneous CSDs with those evoked in a minimally invasive manner by using optogenetics through the intact skull. In total, five spontaneous CSD events (three in *Cacna1a*^{R192Q} and two in *Cacna1a*^{S218L} mice) were observed in 7 days of recording of 10 mice per genotype, whereas no such events were observed in WT mice. In CSD-free periods, FHM1 mutants had an increased ECoG γ-power compared to WT mice, indicative of a state of cortical hyperexcitability that can explain why the mutant mice may be prone to spontaneous CSD events. Several similarities were observed between spontaneous and optogenetically induced CSD events: (1) multiple-wave events were only observed in *Cacna1a*^{S218L} mice; (2) recovery of post-CSD cortical MUA was faster in *Cacna1a*^{S218L} mice; (3) CSD events were accompanied by a combination of behaviours, such as

full body stretching, slow head turning, and rotating body movements, with the latter occurring only with CSD events in mutant mice; and (4) CSD susceptibility was higher during non-REM sleep compared to waking. Furthermore, CSD optogenetically induced in the M1 cortex in FHM1 mutant mice showed a lower induction threshold and a higher propagation rate compared to WT mice, confirming the higher susceptibility for CSD in mutant mice that is also evident from the observation that spontaneous CSD events were never observed in WT mice. Multiple-wave optogenetically induced CSD events, exclusive to *Cacna1a*^{S218L} mice, were associated with a longer time to recovery of TCEPs compared to that of single-wave CSDs. In addition, multi-wave events resulted in a longer impairment of forepaw grab function that persisted up to 6 min after the end of the last CSD wave in M1 cortex.

This study is the first to report spontaneous CSD events in FHM1 mutant mice in which CSD had previously always been induced via chemical, mechanical or electrical activation of cortical neurons (Chen et al., 2016). The only other FHM1 mouse strain for which spontaneous CSDs had been reported are in-house developed FHM3 mutants that express $Na_V1.1$ channels containing mutated α1 subunits that harbour the human *SCN1A*^{L263V} mutation (Jansen et al., 2020). Spontaneous occurrence of CSD events in FHM1 mutant mice appears to be rarer than seen with heterozygous FHM3 mutant mice in which in one out of three mice multiple spontaneous CSDs per animals were recorded in the first days following surgery (Jansen et al., 2020). In contrast, in FHM1 mutant mice, on average, only one event was observed during a 1-week period in about one-third of animals. Whereas in heterozygous FHM3 mutant mice all observed spontaneous CSDs travelled from the visual cortex to the anterior part of the cortex (Jansen et al., 2020), in FHM1 mutant mice spontaneous CSDs were first detected in either the visual or the motor cortex and in some animals appeared even simultaneously at both locations suggesting a different, likely subcortical, location of origin. Given the different paths of propagation, a direct comparison of the speed of the spontaneous CSD events in FHM1 and FHM3 mice is challenging. For evoked CSDs, however, such comparison is feasible, which revealed that the propagation rate of optogenetically induced CSD events in FHM1 *Cacna1a*^{R192Q} and *Cacna1a*^{S218L} mice ranged between 6 and 8 mm/min (with WT values between 4 and 6 mm/min), whereas the rate of electrically evoked CSDs in FHM3 mutant mice was not different from that in WT mice, hence also between 4 and 6 mm/min (Jansen et al., 2020).

Analyses of long-term recordings in freely behaving mice revealed an increased power in the ECoG γ-band frequency for both V1 and M1 cortex in *Cacna1a*^{R192Q} compared to WT mice, whereas the power in the δ-band was reduced in the mutant M1 cortex during REM and non-REM sleep. These findings indicate that the *Cacna1a* R192Q mutation results in measurable alterations in cortical network activity patterns under freely behaving conditions in both V1 and M1 cortex that may contribute to the occurrence of spontaneous CSD events. Notably, the presence of increased γ-power at the cortical network level suggests an elevated baseline cortical network excitability in the migraine susceptible brain. On top of such baseline hyperexcitability, likely physiological cycles in neuronal activity (as they occur during sleep) together with effects of external stimuli (trigger factors) may occasionally create a condition in which the threshold for initiation of CSD is exceeded in the mutant brain. Neuronal hyperexcitability has indeed been proposed as an underlying mechanism for the increased susceptibility to migraine attacks (Welch et al., 1990; Aurora and Wilkinson, 2007; Vikelis and Mitsikostas, 2007). In agreement with this, gain-of-function FHM1 mutations result in increased calcium entry into pre-synaptic terminals with concomitant increased glutamate release into the synaptic cleft (Van den Maagdenberg et al., 2004; Tottene et al., 2009; Van den Maagdenberg et al., 2010), with apparent little effect on inhibitory neurotransmission (Tottene et al., 2009; Vecchia et al., 2014; Vecchia et al., 2015). Our data indicate that these synaptic changes seem to infer significant changes in network activity patterns and predispose the cortex for occurrence of spontaneous CSD events, adding translational value to the FHM1 mutant mouse model. To further investigate in FHM1 mutant mice cortical network changes underlying the initiation and origin of spontaneous CSD events, as well as the propagation path through the brain, broader electrophysiological mapping using flexible surface or depth arrays of graphene solution-gated field-effect transistors (gSGFETs) (Masvidal-Codina et al., 2021) could provide more insight. Also, combining neurophysiology with novel neurovascular imaging (Bourgeais-Rambur et al., 2022) or monitoring technology (Yousef et al., 2021; Yousef Yengej et al., 2022) in freely behaving FHM1 mutant animals may provide novel opportunities to increase insight in mechanisms underlying the spontaneous initiation of CSDs, as a step towards understanding initiation of spontaneous attacks of migraine with aura in patients.

We and others have shown that optogenetics is a successful CSD induction method that is relatively non-invasive and can easily be used in freely behaving animals (Houben et al., 2017; Chung et al., 2019; Tang et al., 2020; Harriott et al., 2021; Masvidal-Codina et al., 2021; Yousef et al., 2021; Yousef Yengej et al., 2022; Pi et al., 2022; Dehghani et al., 2023). Here, optogenetics was used to assess the threshold and propagation rate of CSD and showed that induction of CSD in *Cacna1a*^{S218L} mice often triggered multiple-wave CSDs that were never observed in *Cacna1a*^{R192Q} or WT mice. The fact that also some of the spontaneous CSDs in *Cacna1a*^{S218L} mice showed multiple-wave CSDs shows that this is a genuine finding. Combined with the prolonged motor function impairment seen with multiple-wave events by the wire grab test in our present work, these observations testify of a more profound behavioural impact of CSD events in case of the S218L missense mutation. Our data from freely behaving heterozygous *Cacna1a*^{S218L} mice complement earlier observations from anesthetized mice that underscore a more pronounced CSD susceptibility phenotype in heterozygous *Cacna1a*^{S218L} compared to homozygous *Cacna1a*^{R192Q} mice. Heterozygous *Cacna1a*^{S218L} mice were shown to display a slightly higher CSD frequency and propagation rate for KCl-induced CSDs (Eikermann-Haerter et al., 2009), and showed a higher propensity of multiple-wave events following a single electrical stimulation (Van den Maagdenberg et al., 2010). The multiple-wave CSD events in *Cacna1a*^{S218L} mutants appear to reflect a high sensitivity of the S218L brain to even mild stimuli, that may also underlie the severe and clinically broad phenotype of S218L patients with prolonged hemiplegic attacks, compared to the pure hemiplegic migraine symptoms in R192Q carriers.

To gain better insight in the impact of CSD on cortical network activity, we next compared the recovery of cortical neuronal multi-unit activity (MUA) after spontaneous and optogenetically induced CSD. For the optogenetic CSD events we also assessed the recovery of transcallosal optogenetically evoked potential (TCEP) responses. Although MUA recovered slowly after CSD – and did not even return to 100% in 1 h –, we found a more complete recovery after optogenetic CSD in *Cacna1a*^{S218L} compared to WT mice during the last 20 min of the 1-h post-CSD recording period. For the spontaneous CSDs, a similar faster MUA recovery was observed for the events in *Cacna1a*^{S218L} compared to those in *Cacna1a*^{R192Q} mice in the 40- to 60-min window after CSD. Where recovery of cortical MUA after CSD was rather slow – taking up to 60 min or longer – recovery of TCEP amplitude after optogenetically induced CSD showed full recovery already within minutes. Compared to single-wave CSDs, multiple-wave CSDs in *Cacna1a*^{S218L} mice were associated with a slightly prolonged impairment of TCEP amplitude, in line with the longer forepaw grab duration observed for multiple-wave events, but both readouts recovered within 6 min after CSD. Timewise, the recovery of cortical evoked responses within minutes following CSD in our study is similar to previously reported recovery of evoked potential amplitudes induced by optogenetic stimulation of the barrel cortex following optogenetically induced CSD (Böhm et al., 2019), however, the reported overshoot of N1 amplitude was not visible in our TCEP recordings. The much longer recovery of MUA – compared to that of TECPs – might be linked to the prolonged reduction of cerebral blood flow observed after CSD in our earlier optogenetic CSD study (Houben

et al., 2017), although the time to recovery was not assessed in detail in the present study. Under anesthesia, cortical blood flow was found to not fully recover within 60 min following optogenetic CSD induction (Böhm et al., 2019), and under freely behaving conditions was described to recover within 30–40 min in the awake state and just under 60 min in mice that were asleep (Yousef Yengej et al., 2022). The observed much faster recovery of evoked responses and motor function after CSD, compared to a prolonged suppression of local MUA and vascular changes, in both WT and mutant mice, indicates that CSD has distinct effects at the local neuronal and vascular level, compared to its effects on the broader brain network function. At a translational level, this seems in line with clinical observations from common migraine with aura, that during the migraine aura phase patients typically only experience mild sensory disturbances instead of a complete suppression of cortical function (Charles, 2018).

Our approach of comparing spontaneous and optogenetically induced CSD allowed us to obtain an in-depth characterization of CSD-related behaviour. The fact that CSD-related behaviours were much alike for both spontaneous and induced CSD, more than anything underscores the value of our optogenetic CSD-induction approach, which has the great advantage that the timing of events is well controlled. The observation of a combination of three identified CSD-associated behaviours, i.e., full body stretching, slow head turning, and one-directional rotating body movements in one unoperated mutant mouse possibly reflects the occurrence of a spontaneously occurring CSD in that animal. Minimally-invasive neurovascular monitoring techniques, such as laser doppler flowmetry (Houben et al., 2017) or microchips for measuring cortical optical intrinsic signals (Yousef et al., 2021), provide useful tools for exploring this further in mutant mouse models displaying spontaneous CSD events.

Previously, chemically or pinprick induced CSD was associated in rats with anxiety and pain-related acute behaviours, such as freezing (defined as a sudden interruption of any behaviour, accompanied by a blank stare), head-shaking, and wet-dog shakes (Akcali et al., 2010; Tepe et al., 2015; Filiz et al., 2019). Such transient freezing behaviour was also observed using optogenetic CSD induction in WT mice, but only when triggered in the awake state, whereas CSD events triggered during sleep seemed accompanied by head rubbing and in a few cases characteristic elongation (likely similar to the stretching observed in our animals) of the body (Yousef Yengej et al., 2022). Hence, the absence of freezing behaviour in relation to the spontaneous CSDs in our FHM1 mutant mice may be due to the predominant occurrence of the observed spontaneous events during sleep, although this does not provide a satisfactorily explanation why we did not observe freezing after optogenetically triggered CSDs in awake mice. Whereas the possibility always remains that some freezing episodes may have been missed due to suboptimal video recording conditions (e.g. eyes not visible), we consider the absence of such behaviour being a genuine finding in our study more likely. Alternatively, experimental conditions, such as differences in animal strains (mice vs rats) or the method of CSD induction (KCl, pinprick, or optogenetic induction) may lead to a difference in the prominence of freezing as CSD-associated behaviour. It is noteworthy though that with respect to optogenetically induced CSD, a longer duration and higher intensity of stimulation, i.e., between 5 and 60 s at a 25-mW LED output, was used to induce CSD in awake mice over the posterior cortex in the study by Yousef Yengej and co-workers (Yousef Yengej et al., 2022), whereas in our study CSD for the behavioural analysis was induced in the V1 cortex using 4-mW pulses that were all below 15 s in duration.

In our earlier study, FHM1 mutant, and not WT, mice after KCl induced CSD showed unilateral motor deficits reflected by local circling movements and leaning behaviour that were interpreted as signs of hemiplegia that occurred within minutes after CSD – other behavioural features were not reported, although admittedly not carefully looked at given the challenges related to recovery from anesthesia (Eikermann-Haerter et al., 2009). Our recent study, in which three CSDs were induced by optogenetics, revealed that FHM1 mutant and WT mice exhibit pain-related behaviours (i.e., increased mouse grimace scale scores, oculotemporal strokes and reduced nest building performance) – some more pronounced in the mutant mice (Dehghani et al., 2023) –, but again no freezing, head-shaking, nor wet-dog shakes.

A compelling explanation as to why FHM1 mutant mice showed characteristic one-directional rotating body movements (combined with full body stretching and/or slow head turning) is difficult to provide. Circular movements have been observed before in species other than mice. Electrical stimulation of striatum induced contralateral head turning and circling behaviour in cats (Buchwald and Ervin, 1957) and rats (Hansing et al., 1968). Moreover, SD elicited in the rat striatum was able to induce contralateral circling (Weiss and Fifkova, 1956; Stille and Sayers, 1969; Jakobartl and Huston, 1977). Motivated by observations of subcortical spread of SD to striatum in a minority of events in WT and almost all events in FHM1 mutant mice – with SDs spreading even further to hippocampus and thalamus in a subset of *Cacna1a*^{S218L} mutant mice – we could demonstrate contralateral rotating body movements, that occurred at the same time as striatal SD, in FHM1 mutant mice. Unfortunately, the relationship between contralateral body rotations and striatal SD occurrence does not appear straightforward since WT mice, which do not show CSD-associated body rotations also show striatal SD events.

A marked similarity between the spontaneous and optogenetically induced CSD events was the apparent enhanced CSD susceptibility during sleep. Not only were the majority of spontaneous CSDs in FHM1 mutants initiated during sleep, but also optogenetical induction of CSD was more easy when mice were in non-REM sleep. The latter is in line with a reduced CSD threshold during sleep compared to waking in mice without an FHM mutation (Yousef Yengej et al., 2022). It is not known whether attacks in patients with hemiplegic migraine occur more often during sleep although one-third report that sleeping 'too much' or 'too little' is a trigger for their attacks in a Danish survey (Hansen et al., 2011). Observations in common migraine, including migraine with aura, seem to suggest that attacks more frequently occur in the early morning, i.e., in the context of awakening from sleep, possibly triggered by sleep disturbances (Poulsen et al., 2021). Such clinical observations may be interpreted as a build-up of attack susceptibility during sleep, that would be in line with the enhanced CSD susceptibility during sleep observed in the mouse experiments. Still a direct comparison between species is compromised by the fact that, unlike in humans, in mice, who are nocturnal animals, sleep is fragmented and occurs not only in the light but also in the dark period when mice are active.

Although the ease to induce CSD may vary across vigilance states, we could show that the CSD threshold and propagation rate seems stable (and consequently higher in *Cacna1a*^{S218L} mutant than WT mice) over a number of days. The stability in CSD features over time we observed, contradicts findings of a reduction in propagation rate and duration over time following daily CSD induction (Sukhotinsky et al., 2011). Likely the conventional CSD induction methods used, which entail re-anesthetizing animals for each CSD and reopening burr holes in the skull in case of chemical stimulation (Sukhotinsky et al., 2011) or attaching tubing to craniotomies that are sealed and reopened during freely behaving experiments (Tepe et al., 2015), contribute to this discrepancy. In line with our findings, in a more recent study using microchips glued to the skull for CSD detection optogenetic CSD thresholds were found to be consistent for weeks (Yousef Yengej et al., 2022). Notably, repeated CSD induction, every other day over a 2-week period, in WT mice led to a transient reduction in facial allodynia and increased mouse grimace scale scores (Harriott et al., 2021). Future studies have to show whether induction of repetitive CSDs might have effects on spontaneous CSD events, allodynia, and mouse grimace scale scores in FHM1 mutants.

In conclusion, our study demonstrates that rare spontaneous CSD events in FHM1 mutant mice occur and that optogenetically induced CSDs in the animals show similar behavioural characteristics consisting

of full body stretching, one-directional slow head turning and rotating body movements. Where the majority of spontaneous CSDs occurred during sleep, we were able to demonstrate that optogenetic CSD thresholds were lower during non-REM sleep compared to the awake state as well. The more severe phenotype of the *Cacna1a*^{S218L} mice was associated with the occurrence of multiple-wave CSDs, that were never recorded in *Cacna1a*^{R192Q} and WT mice that only exhibited single-wave CSDs. Multiple-wave CSDs resulted in a more profound CSD-related dysfunction evident as longer suppression of cortical evoked responses and impaired forepaw grip performance. Taken together, our data provide novel insight into mechanisms and features of the spontaneous initiation of CSD that we feel is of value for understanding mechanisms of the migraine aura, as well as for understanding mechanisms of SD in the context of other neurological disorders. In addition, our data provide evidence for the use of optogenetics as a reliable and minimally invasive CSD induction method that induces CSDs with similar characteristics as spontaneously occurring CSDs.

Supplementary data to this article can be found online at https://doi.org/10.1016/j.nbd.2024.106405.

CRediT authorship contribution statement

Inge C.M. Loonen: Data curation, Formal analysis, Investigation, Methodology, Validation, Visualization, Writing – original draft, Writing – review & editing. **Rob A. Voskuyl:** Data curation, Formal analysis, Investigation, Methodology, Writing – review & editing. **Maarten Schenke:** Data curation, Formal analysis, Investigation, Methodology. **Sandra H. van Heiningen:** Data curation, Formal analysis, Investigation, Methodology. **Arn M.J.M. van den Maagdenberg:** Conceptualization, Data curation, Funding acquisition, Project administration, Resources, Supervision, Writing – original draft, Writing – review & editing. **Else A. Tolner:** Conceptualization, Data curation, Funding acquisition, Methodology, Project administration, Resources, Software, Supervision, Writing – original draft, Writing – review & editing.

Declaration of competing interest

The authors have no financial conflicts of interest associated with the work presented in this manuscript.

Data availability

The datasets generated during and/or analysed during the current study are available from the corresponding author on reasonable request.

Acknowledgements

We thank Drs. Thijs Perenboom and Dr. Mark van de Ruit for assistance with data analysis, Imke Steensma for assistance with histology and genotyping, and Prof. dr. Jelle Goeman for his advice on the statistics used in this study. This work was supported by the European Union's (EU) Seventh Framework program "EUROHEADPAIN" (nr. 602633 to A.M.J.M.v.d.M.), an LUMC Fellowship and Marie Curie Career Integration Grant (to E.A.T), the European Innovation Council EIC Pathfinder Programme Project MICROVASC (nr 101070917 to A.M.J.M.v.d.M.), the ZonMw funded JPND Grant "REBALANCE" (nr JPND2022-100 to A.M.J.M.v.d.M.) and the Medical Delta program "Medical NeuroDelta: Ambulant Neuromonitoring for Prevention and Treatment of Brain Disease" (to A.M.J.M.v.d.M.).

References

Akcali, D., Sayin, A., Sara, Y., Bolay, H., 2010. Does single cortical spreading depression elicit pain behaviour in freely moving rats? Cephalalgia 30, 1195–1206. https://doi.org/10.1177/0333102409360828.

Ashina, H., Christensen, R.H., Ashina, M., 2022. Provoked versus spontaneous migraine attacks: pathophysiological similarities and differences. J. Headache Pain 23, 87. https://doi.org/10.1186/s10194-022-01464-2.

Aurora, S.K., Wilkinson, F., 2007. The brain is hyperexcitable in migraine. Cephalalgia 27, 1442–1453. https://doi.org/10.1111/j.1468-2982.2007.01502.x.

Ayata, C., 2013. Pearls and pitfalls in experimental models of spreading depression. Cephalalgia 33, 604–613. https://doi.org/10.1177/0333102412470216.

Böhm, M., Chung, D.Y., Gómez, C.A., Qin, T., Takizawa, T., Sadeghian, H., 2019. Neurovascular coupling during optogenetic functional activation: local and remote stimulus-response characteristics, and uncoupling by spreading depression. J. Cereb. Blood Flow Metab. 40, 808–822. https://doi.org/10.1177/0271678X19845934.

Bourgeais-Rambur, L., Beynac, L., Mariani, J.C., Tanter, M., Deffieux, T., Lenkei, Z., Villanueva, L., 2022. Altered cortical trigeminal fields excitability by spreading depolarization revealed with in vivo functional ultrasound imaging combined with electrophysiology. J. Neurosci. 42, 6295–6308. https://doi.org/10.1523/JNEUROSCI.1825-21.2022.

Buchwald, N.A., Ervin, F.R., 1957. Evoked potentials and behavior: a study of responses to subcortical stimulation in the awake, unrestrained animal. Electroencephalogr. Clin. Neurophysiol. 9, 477–496. https://doi.org/10.1016/0013-4694(57)90036-6.

Chan, Y.C., Burgunder, J.M., Wilder-Smith, E., Chew, S.E., Lam-Mok-Sing, K.M., Sharma, V., Ong, B.K., 2008. Electroencephalographic changes and seizures in familial hemiplegic migraine patients with the CACNA1A gene S218L mutation. J. Clin. Neurosci. 15, 891–894. https://doi.org/10.1016/j.jocn.2007.01.013.

Charles, A., 2018. The migraine aura. Continuum (Minneap Minn) 24, 1009–1022. https://doi.org/10.1212/CON.0000000000000627.

Chen, S.P., Tolner, E.A., Eikermann-Haerter, K., 2016. Animal models of monogenic migraine. Cephalalgia 36, 704–721. https://doi.org/10.1177/0333102416645933.

Chung, D.Y., Sadeghian, H., Qin, T., Lule, S., Lee, H., Karakaya, F., Goins, S., Oka, F., Yaseen, M.A., Houben, T., Tolner, E.A., van den Maagdenberg, A.M.J.M., Whalen, M. J., Sakadžic, S., Ayata, C., 2019. Determinants of Optogenetic cortical spreading depolarizations. Cereb. Cortex 309 (3), 1150–1161. https://doi.org/10.1093/cercor/bhy021. PMID: 29425263; PMCID: PMC6373833.

Dehghani, A., Schenke, M., van Heiningen, S.H., Karatas, H., Tolner, E.A., van den Maagdenberg, A.M.J.M., 2023. Optogenetic cortical spreading depolarization induces headache-related behaviour and neuroinflammatory responses some prolonged in familial hemiplegic migraine type 1 mice. J. Head. Pain 24, 96–111. https://doi.org/10.1186/s10194-023-01628-8.

Dreier, J.P., 2011. The role of spreading depression, spreading depolarization and spreading ischemia in neurological disease. Nat. Med. 17, 439–447. https://doi.org/10.1038/nm.2333.

Dreier, J.P., Reiffurth, C., 2015. The stroke-migraine depolarization continuum. Neuron 86, 902–922. https://doi.org/10.1016/j.neuron.2015.04.004.

Eikermann-Haerter, K., Dileköz, E., Kudo, C., Savitz, S.I., Waeber, C., Baum, M.J., Ferrari, M.D., van den Maagdenberg, A.M., Moskowitz, M.A., Ayata, C., 2009. Genetic and hormonal factors modulate spreading depression and transient hemiparesis in mouse models of familial hemiplegic migraine type 1. J. Clin. Invest. 119, 99–109. https://doi.org/10.1172/JCI36059.

Eikermann-Haerter, K., Yuzawa, I., Qin, T., Wang, Y., Baek, K., Kim, Y.R., Hoffmann, U., Dilekoz, E., Waeber, C., Ferrari, M.D., van den Maagdenberg, A.M., Moskowitz, M. A., Ayata, C., 2011. Enhanced subcortical spreading depression in familial hemiplegic migraine type 1 mutant mice. J. Neurosci. 31, 5755–5763. https://doi.org/10.1523/JNEUROSCI.5346-10.2011.

Filiz, A., Tepe, N., Eftekhari, S., Boran, H.E., Dilekoz, E., Edvinsson, L., Bolay, H., 2019. CGRP receptor antagonist MK-8825 attenuates cortical spreading depression induced pain behaviour. Cephalalgia 39, 354–365. https://doi.org/10.1177/0333102417735845.

Fisher, S.P., Godinho, S.I., Pothecary, C.A., Hankins, M.W., Foster, R.G., Peirson, S.N., 2012. Rapid assessment of sleep-wake behaviour in mice. J. Biol. Rhythm. 27, 48–58. https://doi.org/10.1177/0748730411431550.

Hansen, J.M., Hauge, A.W., Ahina, M., Olesen, J., 2011. Trigger factors for familial hemiplegic migraine. Cephalalgia 31 (12), 1274–1281. https://doi.org/10.1177/0333102411415878. Epub 2011 Jul 22. PMID: 21784774.

Hansing, R.A., Schwartzbaum, J.S., Thompson, J.B., 1968. Operant behavior following unilateral and bilateral caudate lesion in the rat. J. Comp. Physiol. Psychol. 66, 378–388. https://doi.org/10.1037/h0026318.

Harriott, A.M., Chung, D.Y., Uner, A., Bozdayi, R.O., Morais, A., Takizawa, T., Qin, T., Ayata, C., 2021. Optogenetic spreading depression elicits trigeminal pain and anxiety behavior. Ann. Neurol. 89, 99–110. https://doi.org/10.1002/ana.25926.

Houben, T., Loonen, I.C., Baca, S.M., Schenke, M., Meijer, J.H., Ferrari, M.D., Terwindt, G.M., Voskuyl, R.A., Charles, A., van den Maagdenberg, A.M., Tolner, E. A., 2017. Optogenetic induction of cortical spreading depression in anesthetized and freely behaving mice. J. Cereb. Blood Flow Metab. 37, 1641–1655. https://doi.org/10.1177/0271678X16645113.

Jakobartl, L., Huston, J.P., 1977. Circling and consumatory behavior induced by striatal and neocortical spreading depression. Physiol. Behav. 19, 673–677. https://doi.org/10.1016/0031-9384(77)90042-7.

Jansen, N.A., Dehghani, A., Linssen, M.M.L., Breukel, C., Tolner, E.A., van den Maagdenberg, A.M.J.M., 2020. First FHM3 mouse model shows spontaneous cortical spreading depolarizations. Ann. Clin. Transl. Neurol. 7, 132–138. https://doi.org/10.1002/acn3.50971.

Karatas, H., Erdener, S.E., Gursoy-Ozdemir, Y., Lule, S., Eren-Koçak, E., Sen, Z.D., Dalkara, T., 2013. Spreading depression triggers headache by activating neuronal Panx1 channels. Science 339, 1092–1095. https://doi.org/10.1126/science.1231897.

Kors, E.E., Terwindt, G.M., Vermeulen, F.L., Fitzsimons, R.B., Jardine, P.E., Heywood, P., Love, S., van den Maagdenberg, A.M., Haan, J., Frants, R.R., Ferrari, M.D., 2001. Delayed cerebral edema and fatal coma after minor head trauma: role of the CACNA1A calcium channel subunit gene and relationship with familial hemiplegic migraine. Ann. Neurol. 49, 753–760. https://doi.org/10.1002/ana.1031.

Leao, A.A., 1944. Spreading depression of activity in the cerebral cortex. J. Neurophysiol. 7, 359–390. https://doi.org/10.1152/jn.1944.7.6.359.

Masvidal-Codina, E., Smith, T.M., Rathore, D., Gao, J., Illa, X., Prats-Alfonso, E., Corro, E. D., Calia, A.B., Rius, G., Martin-Fernandez, I., Guger, C., Reitner, P., Villa, R., Garrido, J.A., Guimerà-Brunet, A., Wykes, R.C., 2021. Characterization of optogenetically-induced cortical spreading depression in awake mice using graphene micro-transistor arrays. J. Neural Eng. 18 (5) https://doi.org/10.1088/1741.

Ophoff, R.A., Terwindt, G.M., Vergouwe, M.N., van Eijk, R., Oefner, P.J., Hoffman, S.M., Lamerdin, J.E., Mohrenweiser, H.W., Bulman, D.E., Ferrari, M., Haan, J., Lindhout, D., van Ommen, G.J., Hofker, M.H., Ferrari, M.D., Frants, R.R., 1996. Familial hemiplegic migraine and episodic ataxia type-2 are caused by mutations in the Ca2+ channel gene CACNL1A4. Cell. 87, 543–552. https://doi.org/10.1016/s0092-8674(00)81373-2.

Pi, C., Tang, W., Li, Z., Liu, Y., Jing, Q., Dai, W., Wang, T., Yang, C., Yu, S., 2022. Cortical pain induced by optogenetic cortical spreading depression: from whole brain activity mapping. Mol. Brain 15, 99. https://doi.org/10.1186/s13041-022-00985-w.

Poulsen, A.H., Younis, S., Thuraiaiyah, J., Ashina, M., 2021. The chronobiology of migraine: a systematic review. J. Headache Pain 22::76. https://doi.org/10.1186/s10194-021-01276-w.

Stam, A.H., Luijckx, G.J., Poll-Thé, B.T., Ginjaar, I.B., Frants, R.R., Haan, J., Ferrari, M. D., Terwindt, G.M., van den Maagdenberg, A.M., 2009. Early seizures and cerebral oedema after trivial head trauma associated with the CACNA1A S218L mutation. J. Neurol. Neurosurg. Psychiatry 80, 1125–1129. https://doi.org/10.1136/jnnp.2009.177279.

Stille, G., Sayers, A., 1969. Effect of a striatal spreading depression on the pharmacogenic catatonia. Int. J. Neuropharmacol. 8, 181–189. https://doi.org/10.1016/0028-3908(69)90012-4.

Sukhotinsky, I., Dilekoz, E., Wang, Y., Qin, T., Eikermann-Haerter, K., Waeber, C., Ayata, C., 2011. Chronic daily cortical spreading depressions suppress spreading depression susceptibility. Cephalalgia 31, 1601–1608. https://doi.org/10.1177/0333102411425865.

Tang, C., Unekawa, M., Kitagawa, S., Takizawa, T., Kayama, Y., Nakahara, J., Shibata, M., 2020. Cortical spreading depolarisation-induced facial hyperalgesia, photophobia and hypomotility are ameliorated by sumatriptan and olcegepant. Sci. Rep. 10, 11408. https://doi.org/10.1038/s41598-020-67948-w.

Tepe, N., Filiz, A., Dilekoz, E., Akcali, D., Sara, Y., Charles, A., Bolay, H., 2015. The thalamic reticular nucleus is activated by cortical spreading depression in freely moving rats: prevention by acute valproate administration. Eur. J. Neurosci. 41, 102–108. https://doi.org/10.1111/ejn.12753.

Tolner, E.A., Chen, S.P., Eikermann-Haerter, K., 2019. Current understanding of cortical structure and function in migraine. Cephalalgia 39, 1683–1699. https://doi.org/10.1177/0333102419840643.

Tottene, A., Conti, R., Fabbro, A., Vecchia, D., Shapovalova, M., Santello, M., Maagdenberg, A.M., Ferrari, M.D., Pietrobon, D., 2009. Enhanced excitatory transmission at cortical synapses as the basis for facilitated spreading depression in ca(v)2.1 knockin migraine mice. Neuron 61, 762–773. https://doi.org/10.1016/j.neuron.2009.01.027.

Van den Maagdenberg, A.M., Pietrobon, D., Pizzorusso, T., Kaja, S., Broos, L.A., Ceseti, T., van de Ven, R.C., Tottene, A., van der Kaa, J., Plomp, J.J., Frants, R.R., Ferrari, M.D., 2004. A *Cacna1a* knockin migraine mouse model with increased susceptibility to cortical spreading depression. Neuron 41, 701–710. https://doi.org/10.1016/s0896-6273(04)00085-6.

Van den Maagdenberg, A.M., Pizzorusso, T., Kaja, S., Terpolili, N., Shapovalova, M., Hoebeek, F.E., Barrett, C.F., Gherardini, L., van de Ven, R.C., Todorov, B., Broos, L. A., Tottene, A., Gao, Z., Fodor, M., De Zeeuw, C.I., Frants, R.R., Plesnila, N., Plomp, J.J., Pietrobon, D., Ferrari, M.D., 2010. High cortical spreading depression susceptibility and migraine-associated symptoms in ca(v)2.1 S218L mice. Ann. Neurol. 67, 85–98. https://doi.org/10.1002/ana.21815.

Vecchia, D., Tottene, A., van den Maagdenberg, A.M.J.M., Pietrobon, D., 2014. Mechanism underlying unaltered cortical inhibitory synaptic transmission in contrast with enhanced excitatory transmission in $Ca_V2.1$ knockin migraine mice. Neurobiol. Dis. 69, 225–234. https://doi.org/10.1016/j.nbd.2014.05.035.

Vecchia, D., Tottene, A., van den Maagdenberg, A.M.J.M., Pietrobon, D., 2015. Abnormal cortical synaptic transmission in CaV2.1 knockin mice with the S218L missense mutation which causes a severe familial hemiplegic migraine syndrome in humans. Front. Cell. Neurosci. 9, 8. https://doi.org/10.3389/fncel.2015.00008.

Vikelis, M., Mitsikostas, D.D., 2007. The role of glutamate and its receptors in migraine. CNS Neurol. Disord. Drug Targets 6, 251–257. https://doi.org/10.2174/187152707781387279.

Weiss, T., Fifkova, E., 1956. The effect of neocortical and caudatal spreading depression on “circling movements” induced from the caudate nucleus. Physiol. Bohemoslov. 12, 33–38 (PMID: 14060621).

Welch, K.M., D’Andrea, G., Tepley, N., Barkley, G., Ramadan, N.M., 1990. The concept of migraine as a state of central neuronal hyperexcitability. Neurol. Clin. 8, 817–828 (PMID: 1979655).

Yousef Yengej, D., Nwaobi, S.E., Ferando, I., Kechechyan, G., Charles, A., Faas, G.C., 2022. Different characteristics of cortical spreading depression in the sleep and wake states. Headache 65, 577–587. https://doi.org/10.1111/head.14300.

Yousef, Yengej D., Ferando, I., Kechechyan, G., Nwaobi, S.E., Raman, S., Charles, A., Faas, G.C., 2021. Continuous long-term recording and triggering of brain neurovascular activity and behaviour in freely moving rodents. J. Physiol. 599, 4545–4559. https://doi.org/10.1111/head.14300.

Zhang, X., Levy, D., Noseda, R., Kainz, V., Jakubowski, M., Burstein, R., 2010. Activation of meningeal nociceptors by cortical spreading depression: implications for migraine with aura. J. Neurosci. 30, 8807–8814. https://doi.org/10.1523/JNEUROSCI.0511-10.2010.

Zhang, X., Levy, D., Kainz, V., Noseda, R., Jakubowski, M., Burstein, R., 2011. Activation of central trigeminovascular neurons by cortical spreading depression. Ann. Neurol. 69, 855–865. https://doi.org/10.1002/ana.22329.